

# Dissipative quantum phase transitions in ion traps

Malte Darling Dueholm

March 13th 2015

## Preface

This thesis ...

## **English summary**

This thesis ...

## Danske resume

This thesis ...

# Contents

<b>Contents</b>	<b>1</b>
<b>1 Introduction</b>	<b>3</b>
<b>2 Fundamentals</b>	<b>5</b>
2.1 From classical mechanics to quantum mechanics . . . . .	5
2.2 State vectors . . . . .	6
2.3 Observables . . . . .	6
2.4 Wave functions . . . . .	7
2.5 Time evolution . . . . .	8
2.6 Quantization of the electromagnetic field . . . . .	10
<b>3 Open system Dicke model</b>	<b>12</b>
3.1 Ion Traps . . . . .	12
3.2 Open systems . . . . .	15
3.3 The Dicke model . . . . .	19
3.4 Derivation of Hamiltonian . . . . .	20
<b>4 Standard Dicke Model</b>	<b>25</b>
4.1 Equations of motion for the mean field . . . . .	25
4.2 Phase diagrams . . . . .	32
4.3 Fluctuations and stability of the system . . . . .	45
<b>5 Extended Dicke model</b>	<b>53</b>
5.1 Equations of motion . . . . .	53
5.2 Fluctuations . . . . .	54
5.3 $J_z$ -polynomial . . . . .	55
5.4 Regime 1: $\omega_0 \neq 0$ and $\Omega \neq 0$ . . . . .	56
5.5 Regime 2: $\omega_0 = 0, \epsilon \neq 0$ . . . . .	62
5.6 Regime 3: $\omega_0 = 0, \epsilon = 0$ . . . . .	66

<b>6</b>	<b>The chaotic regime</b>	<b>68</b>
6.1	Chaotic behaviour in small time scales . . . . .	68
6.2	Strange attractors . . . . .	68
<b>7</b>	<b>Conclusion and Outlook</b>	<b>73</b>
7.1	Conclusion . . . . .	73
7.2	Outlook . . . . .	75
<b>A</b>	<b>Mean field equations</b>	<b>77</b>
<b>B</b>	<b>Fluctuations around the mean</b>	<b>82</b>
B.1	Linearization of the noise . . . . .	82
B.2	$\delta\hat{A}, \delta\hat{A}^*$ -terms . . . . .	83
B.3	$\delta\hat{J}_i$ -terms . . . . .	83
B.4	Summary . . . . .	85
<b>C</b>	<b>MATLAB programs</b>	<b>87</b>
	<b>Bibliography</b>	<b>88</b>

# Chapter 1

## Introduction

Since the discovery of quantum mechanics a century ago it has been a task for experimental physicists how to isolate and investigate single quantum systems, but with the invention of the quadrupole mass filter [1] by Wolfgang Paul it was suddenly possible with trapped atoms. Paul's quadrupole mass filter used a set of oscillating potentials to confine ions in two dimensions and with small modifications it has been possible to confine ions in three dimensions. This three dimensional trap is denoted as the Paul trap [2].

With the invention of traps such as the Paul trap and lasers it was now possible to confine and manipulate atoms and Cirac and Zoller implemented a controlled-NOT quantum gate in [3] which was realized experimentally by the NIST group [4]. It was now possible to construct logic gates where one exploits the fact that external and internal states in ion traps can be made to interact by lasers.

The Dicke model [5] is a well known model describing the collective behaviour of  $N$  two-level systems. It has received renewed interest because it exhibits quantum phase transitions and multi-partite entanglement. Phase transitions are well known from nature due to thermal fluctuations [6]. In the limit when the temperature goes to zero these fluctuations disappears, but now quantum fluctuations have an influence on the system and can drive a phase transition, denoted as a quantum phase transition [7] A lot of exciting physics happens in these quantum phase transitions. For instance is symmetry breaking observed, see for instance [8, 9, 10] in phase transitions in the Dicke model. Symmetry broken states are a paradigm of condensed matter physics [6, 11] and are of great interest.

Reiter and Sørensen have in [12] derived an effective operator formalism,

which allows the user to exploit adiabatic elimination of the excited levels to get an effective dissipation operator and it is hence possible to engineer the dissipation. This allows one to investigate quantum systems as a function of the dissipation in the same way as a function of laser detunings, laser strengths, etc.

The starting point of this thesis will be the Dicke model realized in an ion trap and investigate dissipative phase transitions in this system. As an extension to the Dicke model two new concepts are added to the standard Dicke model. The first is sideband cooling in the hope it increases stability and the other is another laser driving which change the dynamics of the system. The aim of this thesis is to produce phase diagrams and to characterize the phases and show how experimentalists can make experiments and see whether nature behaves as this thesis predicts. There will hence be a focus on stability and how the stability can be increased in order for the experiments to run more easily.

The outline of this thesis is

**Chapter 1:** Presents the motivation behind this thesis along with the general outline.

**Chapter 2:** Introduces necessary background information from quantum mechanics and quantum optics.

**Chapter 3:** Introduces the reader to ion traps and a mathematical description of open system and shows the derivation of the Hamiltonian describing the system under investigation.

**Chapter 4:** Describes the tools developed for this thesis and presents results of the standard Dicke model.

**Chapter 5:** Uses the tools developed in chapter 5 and presents results of the extended Dicke model.

**Chapter 6:** Goes into further detail of the chaotic phase seen in chapter 5+6.

**Chapter 7:** Concludes on the findings from chapter 5-7 and discusses further options for the work started with this thesis.

# Chapter 2

## Fundamentals

In this chapter relevant elements from quantum mechanics and quantum optics will be presented. First a short introduction on the transition from classical mechanics to quantum mechanics. This will be followed by a short introduction to key elements from quantum mechanics and the chapter will finally be ended with a quantization of the electromagnetic field.

### 2.1 From classical mechanics to quantum mechanics

In classical mechanics a particle of mass  $m$  constrained to move in a definite direction and subject to a specified force  $F(x, t)$  will move in a deterministic way, which makes it possible to determine its position at all times if we know the initial conditions [13]. In quantum mechanics this determinism disappears and one is left with state vectors, which describe the possible outcomes of for instance position. Quantum mechanics forbids the observer to know the position *and* velocity at *the same time* (in opposition to Newtonian mechanics) due to Heisenberg's uncertainty principle [13]

$$\Delta x \Delta p \geq \frac{\hbar}{2}, \quad (2.1)$$

where  $\Delta x$  is the uncertainty of the position and  $\Delta p$  is the uncertainty of the momentum and  $\hbar$  is Planck's constant.

In the early days of quantum mechanics one treated particles as quantum and the field as semi-classical. This situation is often denoted as the first

quantization [14], where the deterministic description of nature is replaced by state vectors.

## 2.2 State vectors

In quantum mechanics a system is said to be in a given state and the complete knowledge of a system is contained in its state vector  $|\psi\rangle$ , which is an element in the Hilbert space  $\mathcal{H}$ . It is possible to expand this state vector  $|\psi\rangle$  in any orthonormal basis  $\{|n\rangle\}$  of the Hilbert space [15]

$$|\psi\rangle = \sum_n |n\rangle \langle n|\psi\rangle, \quad (2.2)$$

where  $\langle n|\psi\rangle$  often is denoted as  $c_n$  for the projection of  $|\psi\rangle$  on the basis state  $|n\rangle$ . An interpretation of  $c_n$  is that the probability of the system to be in state  $|n\rangle$  is given by  $P_n = |c_n|^2$ . This statistical interpretation of the wave function (or state vector) emphasizes the difference between Newtonian mechanics and quantum mechanics. Another feature of the wave function is the possibility to visualize a quantum state, see section (2.4).

## 2.3 Observables

Observables in quantum mechanics are given by hermitian operators acting on states of the Hilbert space. For an operator  $\hat{O}$  to be hermitian it is required that for any two states  $|\psi_{1,2}\rangle$  in the Hilbert space we have [15]

$$\langle \psi_1 | \hat{O} | \psi_2 \rangle = (\langle \psi_2 | \hat{O} | \psi_1 \rangle)^*. \quad (2.3)$$

The expectation value of the observable  $\hat{O}$  when the system is in the state  $|\psi\rangle$  is

$$\langle \hat{O} \rangle = \langle \psi | \hat{O} | \psi \rangle. \quad (2.4)$$

A special case is when the operator  $\hat{O}$  is diagonal in the basis  $\{|n\rangle\}$ , where the following applies

$$\hat{O}|\psi\rangle = O_\alpha|\psi\rangle \quad (2.5)$$

$$\Rightarrow \langle \hat{O} \rangle = \sum_\alpha O_\alpha |c_\alpha|^2 = \sum_\alpha O_\alpha p_\alpha, \quad (2.6)$$

where  $O_n$  denotes the  $n^{\text{th}}$  eigenvalue of the operator  $\hat{O}$  and  $P_n = |c_n|^2$  is the probability to be in state  $n$ .

## 2.4 Wave functions

Another way to represent a quantum state is by the mentioned wave function, which is a representation of the state in position space. The position space is spanned by position eigenkets  $|x'\rangle$  satisfying [13]

$$\hat{x}|x'\rangle = x'|x'\rangle. \quad (2.7)$$

Space is not considered discrete and a given arbitrary state  $|\phi\rangle$  can be expanded as

$$|\phi\rangle = \int_{-\infty}^{\infty} dx |x\rangle \langle x|\phi\rangle \quad (2.8)$$

The expansion coefficient  $\langle x|\phi\rangle$  is called the wave function of the state  $|\phi\rangle$  and is usually denoted  $\psi_\phi(x)$ . A nice treat of the wave function representation is the possibility to visualize a given quantum state. The Fock states (or number states)  $|n\rangle$  is for instance given by [13]

$$\psi_n(x) = \left(\frac{1}{\pi\lambda^2}\right)^{1/4} \frac{1}{\sqrt{2^n n!}} H_n\left(\frac{x}{\lambda}\right) e^{-x^2/2\lambda^2}, \quad (2.9)$$

where  $\lambda = \sqrt{\hbar/\omega}$  and  $H_n(\xi)$  are the Hermite polynomials. The wave function for  $n = 1, 2$  and  $3$  are seen in figure (2.1).

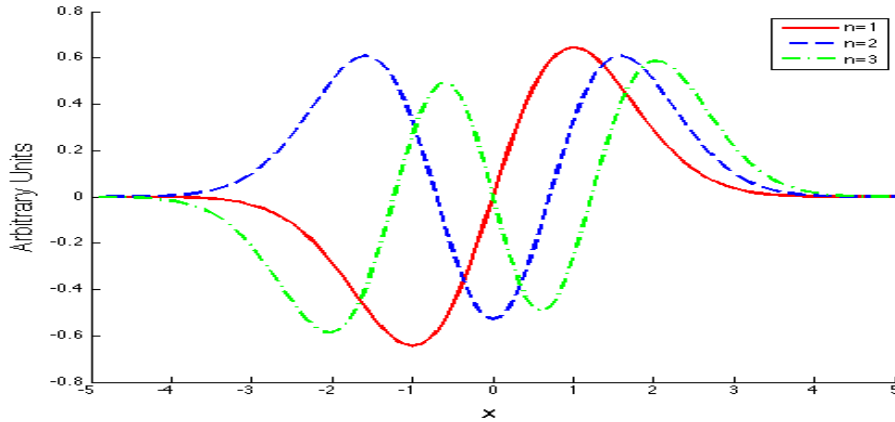


Figure 2.1: The wave functions of the first three Fock states above vacuum.

It is possible to go from the position space to momentum space. The wave function in momentum space  $\psi_\phi(p)$  is obtained from the wave function in position space by a Fourier transform

$$\psi_\phi(p) = \frac{1}{\sqrt{2\pi\hbar}} \int_{-\infty}^{\infty} dx \exp(-ipx/\hbar) \psi_\phi(x). \quad (2.10)$$

## 2.5 Time evolution

There are several ways to introduce time evolution in quantum mechanics and one speaks of which "picture" one observes from. Is it in the Schrödinger's picture where the state vectors evolves in time, in the Heisenberg's picture where the observables evolves in time or in the mixture given by the interaction picture.

### 2.5.1 Schrödinger's picture

In Schrödinger's picture the state vectors evolve in time while the operators remain stationary. The evolution is given by [14, 15]

$$i\hbar \frac{d}{dt} |\psi\rangle = \hat{H} |\psi\rangle, \quad (2.11)$$

where  $|\psi\rangle$  is the state vector of the system and  $\hat{H}$  is the Hamiltonian of the system. The stationary solution of Schrödinger's equation are given by the

vectors  $|E_n\rangle$ , where  $\hat{H}|E_n\rangle = E_n|E_n\rangle$ . It is possible to expand any state in the basis of eigenstates of  $\hat{H}$ . In this case the time evolution of the state vector takes the form [13]

$$|\psi(t)\rangle = \sum_n e^{-iE_n t/\hbar} c_n |E_n\rangle. \quad (2.12)$$

## 2.5.2 Heisenberg's picture

In Heisenberg's picture the operators evolve in time and the state vectors remain stationary, opposite the Schrödinger picture. The observables describing different measurements of the system depends explicitly on the time  $t$  in this picture and evolve according to [14, 15]

$$i\hbar \frac{d}{dt} \hat{O} = [\hat{O}, \hat{H}] + i\hbar \frac{\partial \hat{O}}{\partial t}. \quad (2.13)$$

## 2.5.3 The interaction picture

The interaction picture is also referred to as the Dirac picture, which is an intermediate representation of Schrödinger's and the Heisenberg's pictures. In the interaction picture both the operators and the state vectors carry part of the time dependence of observables (in opposition to Schrödinger's and Heisenberg's picture where one of them was stationary). In order to switch to the interaction picture, the Schrödinger picture Hamiltonian is divided into [15]

$$\hat{H}_S = \hat{H}_{0,S} + \hat{H}_{1,S}, \quad (2.14)$$

where the  $\hat{H}_{0,S}$  often is well understood and exactly solvable, and  $\hat{H}_{1,S}$  is a perturbation to the system. Often eventual explicit time dependence is connected to  $\hat{H}_{1,S}$  such that  $\hat{H}_{0,S}$  is time independent.

The state vectors evolve according to [15]

$$|\Psi_I(t)\rangle = e^{i\hat{H}_{0,S}t/\hbar} |\Psi_S(t)\rangle, \quad (2.15)$$

where  $|\Psi_S(t)\rangle$  is the state vector in the Schrödinger picture. The operators evolve according to

$$\hat{A}_I(t) = e^{i\hat{H}_{0,S}t/\hbar} \hat{A}_S(t) e^{-i\hat{H}_{0,S}t/\hbar} \quad (2.16)$$

The Hamiltonian operator in the interaction picture consists as mentioned of two parts. The first (unperturbed) part  $\hat{H}_{0,I}(t)$  is equal to the Schrödinger equivalent  $\hat{H}_{0,S}(t)$ , while the second part equals

$$\hat{H}_{1,I}(t) = e^{i\hat{H}_0, st/\hbar} \hat{H}_{1,S} e^{-i\hat{H}_0, st/\hbar}. \quad (2.17)$$

The time evolution of state vectors, operators and the density matrix in the interaction picture is given by [15]

$$i\hbar \frac{d}{dt} |\psi_I(t)\rangle = \hat{H}_{1,I}(t) |\psi_I(t)\rangle \quad (2.18)$$

$$i\hbar \frac{d}{dt} \hat{A}_I(t) = [\hat{A}_I(t), \hat{H}_0] \quad (2.19)$$

$$i\hbar \frac{d}{dt} \rho_I(t) = [\hat{H}_{1,I}(t), \rho_I(t)], \quad (2.20)$$

where  $\rho$  is the density matrix, which will be introduced more thoroughly in chapter 3.

## 2.6 Quantization of the electromagnetic field

In the start of quantum mechanics the field was left with a classical description, but with Dirac's ideas from 1927 [16] the a method to describe the quantum field was developed and this quantization is denoted as the second quantization. Light is electromagnetic waves propagating through space and can be treated as small wave packets of energy called photons. These photons can be treated mathematically as energy eigenstates of a harmonic oscillator of unit mass. The Hamiltonian for the single mode electric field in the case of no sources of radiation is [14]

$$\hat{H} = \frac{1}{2} (\hat{p}^2 + \omega^2 \hat{q}^2), \quad (2.21)$$

where  $\hat{p}$  is the canonical momentum operator and  $\hat{q}$  is the canonical position operator. The operators  $\hat{q}$  and  $\hat{p}$  are hermitian operators and hence correspond to observable quantities (position and momentum), but it is often convenient to combine  $\hat{q}$  and  $\hat{p}$  to define two non-hermitian operators called the annihilation and creation operators

$$\hat{a} = \frac{1}{\sqrt{2\hbar\omega}} (\omega\hat{q} + i\hat{p}) \quad (2.22)$$

$$\hat{a}^\dagger = \frac{1}{\sqrt{2\hbar\omega}} (\omega\hat{q} - i\hat{p}). \quad (2.23)$$

Introducing these operators, the Hamiltonian from equation (2.21) can be written as

$$\hat{H} = \hbar\omega \left( \hat{a}^\dagger \hat{a} + \frac{1}{2} \right). \quad (2.24)$$

The eigenstates of the Hamiltonian are called Fock states and are denoted  $|n\rangle$ . They have energy  $E_n$  such that

$$\hat{H}|n\rangle = E_n|n\rangle, \quad (2.25)$$

where

$$E_n = \hbar\omega \left( n + \frac{1}{2} \right), \quad n = 0, 1, 2, \dots \quad (2.26)$$

It follows from equation (2.26) that  $n$  is the number of energy quanta ( $\hbar\omega$ ) contained in the state  $|n\rangle$ , which is equivalent to the number of photons. It is also seen that vacuum ( $n = 0$ ) has the zero point energy  $\frac{1}{2}\hbar\omega$ . The set of all Fock states ( $\{|n\rangle\}$ ) is an orthonormal basis of the Hilbert space of the Hamiltonian (equation (2.21)). It is furthermore a complete set, which means that any state of a single mode electromagnetic field can be written as a superposition of Fock states. When the annihilation/creation operators  $\hat{a}$  ( $\hat{a}^\dagger$ ) acts on a state  $|n\rangle$  one obtains [14]

$$\hat{a}|n\rangle = \sqrt{n}|n-1\rangle \quad (2.27)$$

$$\hat{a}^\dagger|n\rangle = \sqrt{n+1}|n+1\rangle. \quad (2.28)$$

From this it also follows why the  $\hat{a}$  operator is denoted the annihilation operator, since the number of photons  $n$  is reduced by one and why the  $\hat{a}^\dagger$  is denoted the creation operator, since the number of photons is increased by one. Another important operator is the number operator  $\hat{n} = \hat{a}^\dagger \hat{a}$  with the expectation value [13]

$$\langle n|\hat{n}|n\rangle = n. \quad (2.29)$$

$n$  is hence the average number of photons.

# Chapter 3

## Open system Dicke model

This chapter presents initially what ion traps are, how they are constructed and their purpose in quantum computing along with an introduction to the formalism used to describe ions throughout this thesis. Secondly open systems are treated and how they mathematically can be described with the master equation. Thirdly the *standard* Dicke model (what is meant by standard will become clear later) will be presented with focus on *why* the Dicke model is interesting to investigate. The last part is a derivation of the Hamiltonian for the Dicke model.

### 3.1 Ion Traps

An ion trap is an electromagnetic device for confining a charged particle in space. A trapped ion contains two separable quantum systems: a ladder of harmonic oscillator motional states and an internal electronic state (as long the ion is kept undisturbed) [17]. A key feature of the ion trap is that these external and internal states can interact through laser radiation. This section describes briefly how ion traps are constructed, their benefits as the basis for quantum computing and a description of the dynamics in a ion trap.

Ions have a charge and one are hence able to fix its position with electric fields. Furthermore the internal states are insensitive to electric fields and the ions are (almost) fixed in their position while the internal states store information. This section will initially describe key elements for the ion trap and how it can be used in quantum computing. The last part of this section introduces a formalism for two-level ions and how they can be treated mathematically.

### 3.1.1 The force on ions in an electric field

Ions respond strongly to applied electric fields due to the Coulomb interaction [2, 15]. An ion with a single charge  $e = 1.6 \cdot 10^{-19}$  C in an electric field of  $10^5 \text{ Vm}^{-1}$  experiences a force

$$F_{\text{ion}} = eE \approx 10^{-14} \text{ N}, \quad (3.1)$$

which corresponds to 500 V between electrodes which are 5 mm apart. In comparison a neutral atoms with a magnetic moment of one Bohr magneton in a magnetic field gradient of  $\text{dB}/\text{dz} = 10 \text{ Tm}^{-1}$  experiences a force of magnitude [2].

$$F_{\text{neutral}} = \mu_{\text{B}} \left| \frac{\text{dB}}{\text{dz}} \right| \approx 10^{-22} \text{ N}. \quad (3.2)$$

An ion is hence trapped by a force  $10^8$  times greater than magnetically trapped neutrals. The trap depth of such an ion trap corresponds to the kinetic energy of temperature of  $6 \cdot 10^6$  K compared to a trap depth of 0.07 K of neutral atoms [2] which makes it possible to construct extremely tight traps. Furthermore one doesn't need to cool ions as needed for neutral atoms before one can trap them.

### 3.1.2 Earnshaw's theorem

The interaction with electric fields make ions tempting to use, but a charged particle *cannot* rest in stable equilibrium in an electric field [2]. This is known as *Earnshaw's theorem* and it is thus not possible to confine an ion only with electromagnetic fields. This comes from the Laplace equation  $\nabla^2\Phi = 0$ , where  $\Phi$  is the electrostatic potential. A stable trap requires that the potential energy  $U$  has a minimum, i.e.  $\nabla U = 0$  and  $\nabla^2 U > 0$ , but the potential energy is proportional to the electrostatic potential  $U = q\Phi$  and it is hence impossible to make a trap using electrostatic fields. The solution is to introduce time varying fields and the two main ion traps to go to are Penning traps and Paul traps, where this thesis focuses on a Paul trap. The Paul trap has the disadvantage that it exhibit *micromotion* which will be neglected in this thesis [17].

### 3.1.3 The Paul trap

The Paul trap can be illustrated as a rotating saddle-shaped surface. If one picture the ion to be positioned on a saddle-point and able to move a

small perturbation will force the ion to move down the saddle and the ion is hence *not* trapped. If one instead starts to rotate the saddle, the ion will continuously starts to move down in one direction just to moved in the opposite direction a quarter rotation of the saddle later and hence stay fixed around the induced equilibrium. The velocity and hence kinetic energy of the ion depends on how far away from equilibrium the ion moves [2].

### 3.1.4 Resolved sideband cooling

Trapped ions have both internal states of the ions and external states of vibrational modes. It is hence possible for the ions to absorb light at the angular frequency of the transition of the free ion  $\omega_0$  and also the frequencies  $\omega_L = \omega_0 \pm n\omega_v$ , where  $n$  is an integer. This corresponds to transition in which the vibrational motion of the ion changes. The energy of the system is reduced if one uses a laser with the frequency  $\omega_L = \omega_0 - \omega_v$  to excite the first sideband of lower frequency. The vibrational level is hence reduced by one (the new vibrational level equals  $v' = v - 1$ ). The sideband cooling continues until the ion has been driven into its lowest vibrational energy level. It is possible by measurements of the ratio of the sidebands to estimate in which level the ion is in [2].

### 3.1.5 Ion traps and quantum computation

The ion trap was first proposed for quantum computing by Cirac and Zoller [3]. The internal states of the ions (for instance two hyperfine structure states) are shielded from the surroundings and can represent an effective two-level system:  $|0\rangle \leftrightarrow |1\rangle$ . The Pauli operators are suited for describing this two-level system, as introduced in section (3.1.6). To implement the gates between the bits, it was proposed to apply laser fields to the trapped ions. Due to the recoil of an ion upon absorption of a photon both the internal and motional states of the ions are coupled and one can implement gates between the ions [17]. This thesis initially investigate a system where the number of ions goes to infinity  $N \rightarrow \infty$  and the Hamiltonian of the system is presented in section (3.4), but will not go further into how ion traps can be used to quantum computation.

### 3.1.6 Formalism: Ions

Initially a system of a single two-level ion with states  $|g\rangle$  and  $|e\rangle$  is investigated. The ion part is conveniently described by the operators [13]

$$\hat{\sigma}_z = \frac{1}{2} (|e\rangle\langle e| - |g\rangle\langle g|), \quad \hat{\sigma}_+ = |e\rangle\langle g|, \quad \hat{\sigma}_- = |g\rangle\langle e| \quad (3.3)$$

$$\hat{\sigma}_x = \frac{1}{2} (\hat{\sigma}_+ + \hat{\sigma}_-), \quad \hat{\sigma}_y = \frac{i}{2} (\hat{\sigma}_- - \hat{\sigma}_+), \quad (3.4)$$

where the physical interpretation of the operators is that  $\hat{\sigma}_z$  is the population difference between excited and ground state and the  $\hat{\sigma}_\pm$  are the raise and decrease operators between the ground and excited state. These operators satisfy the spin-1/2 algebra of Pauli matrices, i.e.,

$$[\hat{\sigma}_{-,m}, \hat{\sigma}_{+,n}] = -2\hat{\sigma}_{z,m}\delta_{m,n} \quad (3.5)$$

$$[\hat{\sigma}_{-,m}, \hat{\sigma}_{z,n}] = \hat{\sigma}_{-,m}\delta_{m,n} \quad (3.6)$$

$$[\hat{\sigma}_{i,m}, \hat{\sigma}_{j,n}] = \sum_k i\epsilon_{ijk}\hat{\sigma}_{k,m}\delta_{m,n}. \quad (3.7)$$

It is also possible to investigate the entire system using the collective angular momentum operators  $\hat{J}_i, i \in \{x, y, z, \pm\}$ , defined as  $\hat{J}_i = \sum_m \hat{\sigma}_{i,m}$  [18]. These operators do also satisfy the spin-1/2 algebra of Pauli matrices, i.e.

$$[\hat{J}_i, \hat{J}_j] = \sum_{m,n} [\hat{\sigma}_{i,m}, \hat{\sigma}_{j,n}] = \sum_{m,n} \sum_k i\epsilon_{ijk}\hat{\sigma}_{k,m}\delta_{m,n} = \sum_k i\epsilon_{ijk}\hat{J}_k. \quad (3.8)$$

$\hat{J}_z$  is an eigenfunction of the product state  $|\Psi\rangle = |s_1, m_1\rangle|s_2, m_2\rangle \cdots |s_N, m_N\rangle$  with eigenvalues  $m_n$ :

$$\hat{J}_z|\Psi\rangle = \left[ \sum_n m_n \right] |\Psi\rangle. \quad (3.9)$$

The total spin of the system is assumed to be as large as possible  $J \equiv \sum_{n=1}^N s_n = \frac{N}{2}$ , since all the ions can be described as a spin-1/2-system. The eigenvalues of the  $n^{\text{th}}$  ion are given by  $S_{n,\pm}|s, m_n\rangle = \sqrt{(s \mp m_n)(s + 1 \pm m_n)}|s, m_n \pm 1\rangle$  [13].

## 3.2 Open systems

It is possible to investigate complicated systems more efficiently if one truncates the description to include only the few modes or atomic levels of interest. Our system is not isolated and will hence "speak" with the "environment" or the "reservoir" over which we have no control. In many cases one

wants to develop a formalism where the reservoir could be neglected by eliminating for instance radiation field degrees of freedom while the evolution of the system itself still can be described. This section describes mathematical methods to do so.

### 3.2.1 The density operator

In the previous sections the quantum mechanical system has been represented by the state vector  $|\psi\rangle$  in the Hilbert space. The state vector cannot treat macroscopic objects, it is neither always useful to use this representation. The quantum mechanical system (and classical ensembles as well) can be expressed by the density operator  $\hat{\rho}$  given by [14]

$$\hat{\rho} = \sum_n p_n |\psi_n\rangle \langle \psi_n|. \quad (3.10)$$

If there exists a basis in which  $\hat{\rho} = |\phi\rangle \langle \phi|$  for some state  $|\phi\rangle$ , the system is said to be in a "pure" state and likewise if no such basis exists the system is said to be in a "mixed" state. The density operator has several important properties which applies to all density operators. It must first of all be hermitian  $\hat{\rho} = \hat{\rho}^\dagger$ . Secondly its trace over the orthonormal basis  $\{|n\rangle\}$  must equals one  $\text{Tr}[\hat{\rho}] = \sum_n \langle n|\hat{\rho}|n\rangle = 1$ . Thirdly for pure states the following must be satisfied  $\langle n|\hat{\rho}^2|m\rangle \leq \langle n|\hat{\rho}|m\rangle$ , where  $|n, m\rangle$  are any pure state. Note that the first two follows directly from the probability interpretation and conservation of probability [15].

Expectation values can be calculated directly from the density operator. From equation (cite to equation  $\langle \hat{O} \rangle = \langle \psi|\hat{O}|\psi\rangle$  in fundamentals) it follows that

$$\langle \hat{O} \rangle = \sum_\alpha p_\alpha \langle \psi_\alpha | \hat{O} | \psi_\alpha \rangle \quad (3.11)$$

$$= \sum_{\alpha, n} p_\alpha \langle \psi_\alpha | \hat{O} | n \rangle \langle n | \psi_\alpha \rangle \quad (3.12)$$

$$= \sum_n \langle n | \underbrace{\left( \sum_\alpha p_\alpha |\psi_\alpha\rangle \langle \psi_\alpha| \right)}_{\hat{\rho}} | n \rangle \hat{O} | n \rangle \quad (3.13)$$

$$= \text{Tr}[\hat{\rho} \hat{O}] \quad (3.14)$$

The density matrix can also be written such that [15]

$$\hat{\rho} = \sum_{n,n'} |n\rangle \underbrace{\langle n|\hat{\rho}|n'\rangle}_{\rho_{n,n'}} \langle n'| \quad (3.15)$$

where the physical interpretation of the density operator is clear. The diagonal elements  $\rho_{nn} = \langle(|n\rangle\langle n|)\rangle$  correspond to the probability of occupying state  $|n\rangle$  and off-diagonal elements  $\rho_{nm} = \langle(|n\rangle\langle m|)\rangle$ , where  $n \neq m$  correspond to the expectation value of the coherence between level  $|n\rangle$  and  $|m\rangle$ .

### 3.2.2 System and environment

A physical system will often be linked to an environment and one can treat the system and environment as two subsystem of the entire system. The density operator formalism is suited for describing the case where you only care about one of the systems. The entire system given by the state vector  $|\psi\rangle$  with corresponding density operator  $\hat{\rho} = |\psi\rangle\langle\psi|$ . The entire system can be expressed in terms of its two subparts  $\{|e\rangle, |s\rangle\}$ , where  $|e\rangle$  is the state of the environment and  $|s\rangle$  is the state of the system, so that

$$|\psi\rangle = \sum_{n,e} |s\rangle|e\rangle\langle s, e|\psi\rangle. \quad (3.16)$$

If the expectation value of an operator  $\hat{S}$  which acts only on the system degree of freedom,

$$\langle\hat{S}\rangle = \sum_{s,e} \langle s, e|\hat{S}|\psi\rangle\langle\psi|s, e\rangle \quad (3.17)$$

$$= \sum_s \langle s|\hat{S} \left( \underbrace{\sum_e \langle e|\psi\rangle\langle\psi|e\rangle}_{\hat{\rho}_S} \right) |s\rangle \quad (3.18)$$

$$= \text{Tr}_S[\hat{S}\hat{\rho}_S]. \quad (3.19)$$

If one seeks an expectation value of a system operator, it can be found in terms of the reduced density operator

$$\hat{\rho}_S = \text{Tr}_R [\hat{\rho}]. \quad (3.20)$$

If  $\hat{\rho}_S$  describes an open system  $\hat{\rho}_S = \sum_{\alpha} p_{\alpha} |\psi_{\alpha}^S\rangle\langle\psi_{\alpha}^S|$  is a mixed state. If it is a pure state then the system is *not* open.

### 3.2.3 The dynamics of an open system

The reduced density matrix  $\hat{\rho}_S$  evolves in time. If the Hamiltonian only acts on the system, the reduced density matrix evolves according to

$$i\hbar\dot{\hat{\rho}}_S = \sum_{\alpha} p_{\alpha} \left( i\hbar|\dot{\psi}\rangle\langle\psi| + |\psi\rangle i\hbar\langle\dot{\psi}| \right) \quad (3.21)$$

$$= \frac{1}{i\hbar} \left[ \hat{H}_S, \hat{\rho}_S \right]. \quad (3.22)$$

If one includes interacting terms in the Hamiltonian  $\hat{H}_{SR}$  the dynamics will be more complicated.

#### General formalism

The total Hamiltonian consists of three elements, one for the system  $\hat{H}_S$ , one for the environment  $\hat{H}_R$  and one for the interaction between system and environment  $\hat{H}_{SR}$

$$\hat{H} = \hat{H}_S + \hat{H}_R + \hat{H}_{SR}. \quad (3.23)$$

The total density matrix obeys

$$\dot{\hat{\rho}} = \frac{1}{i\hbar} \left[ \hat{H}, \hat{\rho} \right] \quad (3.24)$$

$$= \frac{1}{i\hbar} \left[ \hat{H}_S + \hat{H}_R + \hat{H}_{SR}, \hat{\rho} \right]. \quad (3.25)$$

If one trace over the reservoir degree of freedom on both sides of the equation one observes that the first term ( $\hat{H}_S$ ) gives us equation (3.22), as if there has not been a reservoir, the trace over the reservoir gives zero due to invariance under cyclic permutations and the interaction needed to be treated for the system in question. For a Markovian reservoir (the system and reservoir is factorizable in short time limits and the system is not affected by the knowledge of earlier observations) [19] it is possible in the Schrödinger picture to obtain the master equation [15]

$$\frac{\Delta \hat{\rho}_S}{\Delta t} = - \sum_k \frac{\gamma_k}{2} \bar{n} \left( \hat{c}_k \hat{c}_k^\dagger \hat{\rho}_c - \hat{c}_k^\dagger \hat{\rho}_S \hat{c}_k \right) + HC \quad (3.26)$$

$$- \sum_k \frac{\gamma_k}{2} (\bar{n} + 1) \left( \hat{c}_k^\dagger \hat{c}_k \hat{\rho}_S - \hat{c}_k \hat{\rho}_S \hat{c}_k^\dagger \right) + HC \quad (3.27)$$

$$+ \frac{1}{i\hbar} \left[ \hat{H}_S, \hat{\rho}_S \right], \quad (3.28)$$

where  $\gamma_k$  is the decay rate to the  $k$ 'th mode,  $\bar{n}$  is the average number of ions (see equation (2.27))  $\hat{c}_k$  is a general system operator and  $\hat{\rho}_S$  is the density matrix of the system.

### 3.3 The Dicke model

The standard Dicke model is composed of  $N$  ions cooperatively interacting with a single radiation field. The term *cooperatively* has to be understood in the way that atomic dipoles interact coherently with the privileged (or single) radiation mode [20]. The Dicke model has had renewed interest due to its quantum phase transitions and the multi-partite entanglement from a simple system, where this thesis focusses on the first part.

In order to have  $N$  atoms (or ions) to interact solely with *one* privileged mode of the radiation field a special environment is required, namely that one mode or frequency must dominate while other frequencies are suppressed. The basic Hamiltonian for the Dicke model is given by [8]

$$\hat{H} = \omega \hat{a}^\dagger \hat{a} + \omega_0 J_z + \frac{V}{\sqrt{J}} \hat{x} J_x \quad (3.29)$$

where  $\hbar = 1$ . The operators  $\hat{a}^\dagger$  and  $\hat{a}$  are the usual creation and annihilation operators for the quantized field, and the collectively atomic operators involved  $J_x$  and  $J_z$  are defined in section (3.1.6).

It is seen from equation (3.29) that two terms compete, namely  $\omega_0 J_z$  and  $V/\sqrt{J} \cdot \hat{x} J_x$ . If  $V = 0$  and the system starts in  $J_z = -N/2$  nothing will change this, but if one cranks up  $V$  the two terms will compete until the interesting continuous quantum phase transition occur where the state is changed from having  $J_z$  to  $J_x$  as the dominant term. An example of this is seen in figure (3.1), but this will more thoroughly be presented in chapter (4).

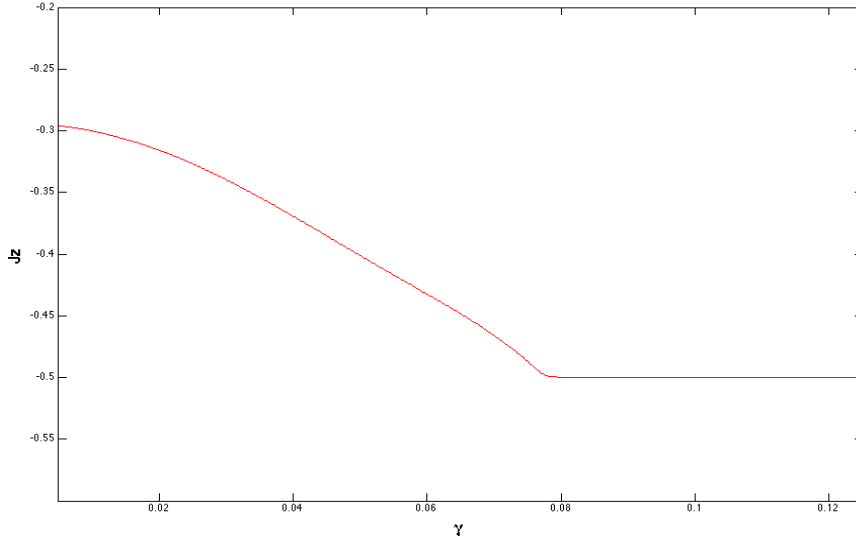


Figure 3.1: A phase transition occurs  $\gamma = \sqrt{(2V^2\omega_0 - \omega\omega_0^2)}/\omega \approx 0.077$ . This figure has been produced with the following parameters:  $\epsilon = 0.0, V = 0.2, \omega = 0.5, \omega_0 = 0.1, \Omega = 0.0$ .

Consistent with for instance [20] a phase transition takes place for  $\gamma$ , when  $\gamma = \sqrt{(2V^2\omega_0 - \omega\omega_0^2)}/\omega$  is found for this model. With the parameters given in the figure text to figure (3.1) the phase transition occur at  $\gamma \approx 0.077$ . The boundary for phase transitions in this model will be presented in section (4.1.3).

### 3.4 Derivation of Hamiltonian

The system under investigation throughout this thesis is an ion-laser system. This system constitute of three separate parts: A part describing the ions with the Hamiltonian  $\hat{H}_{\text{ions}}$ , an electromagnetic part describing the quantized electromagnetic field with the Hamiltonian  $\hat{H}_{\text{field}}$  and the interaction between ions and field  $\hat{H}_{\text{interaction}}$ . This chapter presents the derivation of the Hamiltonian for the extended Dicke model.

Formally the Hamiltonian can be split into the following parts which will be described in the following

$$\hat{H} = \hat{H}_{\text{ions}} + \hat{H}_{\text{field}} + \hat{H}_{\text{interaction}}. \quad (3.30)$$

### 3.4.1 The non-interacting terms

It follows from section (2.6) that the Hamiltonian for the quantized field is given in units of  $\hbar = 1$  by

$$\hat{H}_{\text{field}} = \sum_k^N \omega_k \left( \hat{a}^\dagger \hat{a} + \frac{1}{2} \right) \quad (3.31)$$

or in the case of a single privileged mode with the neglect of zero-point energy

$$\hat{H}_{\text{field}} = \omega \hat{a}^\dagger \hat{a} \quad (3.32)$$

and given the operators presented in section (3.1.6), the Hamiltonian for a single ion can be written as

$$\hat{H}_{\text{ion}} = E_g |g\rangle\langle g| + E_e |e\rangle\langle e| \equiv \frac{\omega_0}{2} \hat{\sigma}_z, \quad (3.33)$$

where the energy of the ground state is given by  $E_g \equiv -\frac{\omega_0}{2}$  and the energy of the excited state is given by  $E_e \equiv \frac{\omega_0}{2}$ , so the zero-energy point is chosen to be directly between the ground and excited state. The energy scheme of the two-level system is illustrated in figure (3.2).

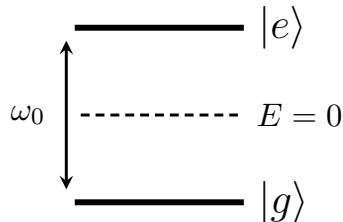


Figure 3.2: The two-level system under investigation.

In this thesis the ions are assumed to be non-interacting and a Hamiltonian for several ions is simply found by taking the sum over the  $N$  ions in the system. The non-interacting term in the Hamiltonian for the ions is hence given by

$$\hat{H}_{\text{ions}} = \frac{\omega_0}{2} \sum_j^N \hat{\sigma}_{z,j} = \frac{\omega_0}{2} \hat{J}_z. \quad (3.34)$$

where the last term originates from the fact that we can use collective angular momentum operators to describe the system.

### 3.4.2 Ion-Light Interaction Term

The last term,  $\hat{H}_{\text{int}}$ , is the ion-light interaction term, which describes the interaction between the ions and the electromagnetic field, where the electromagnetic field is assumed to be uniform across the extension of the point-like atom and the interaction hence can be described by the dipole moment [2].

#### Dipole moment

An electron with charge  $-e$  at a relative position  $\hat{r}$  creates an electric dipole moment  $\hat{d} = -e \cdot \hat{r}$  that couple to the electromagnetic field  $\hat{E}$  at the position of the atom  $\mathbf{r}$ . Formally, the Hamiltonian describing the process is given by [14]

$$\hat{H}_{\text{int}} = \hat{d} \cdot \hat{E}. \quad (3.35)$$

Rewriting this in terms of  $\hat{\sigma}_{\pm}$ -operators one yields [14]

$$\hat{d} = -e \cdot \hat{r} = - \sum_{i,j \in \{e,g\}} e |i\rangle \langle i | \hat{r} | j \rangle \langle j| \stackrel{\mathcal{D}_{i,j} \equiv e \cdot \langle i | \hat{r} | j \rangle}{=} - \sum_{i,j \in \{e,g\}} \mathcal{D}_{i,j} |i\rangle \langle j| \quad (3.36)$$

$$= -\mathcal{D}_{e,g} \hat{\sigma}_- \mathcal{D}_{g,e} \hat{\sigma}_- = -(\mathcal{D}^+ \hat{\sigma}_+ + \mathcal{D}^- \hat{\sigma}_-), \quad (3.37)$$

where the electric dipole moment transition matrix elements  $\mathcal{D}_{i,j}$  ( $i, j \in \{e, g\}$ ) was introduced.

#### Considered system

In the system under investigation, two lasers will drive the  $|g\rangle \leftrightarrow |e\rangle$ -transition detuned with the frequency  $\pm\omega$  from the resonance frequency  $\omega_0$ ,  $\omega_L = \omega_0 \pm \omega$ . Another small detuning of the lasers  $\chi$  is added in order to make sideband cooling of the system. The sideband cooling origin in the fact that the  $\omega_2$  frequency is closer to resonance than  $\omega_1$ , see figure (3.3) for the system under consideration.

The laser fields are characterized by

$$E_1 = \frac{E_0}{2} \exp(-i\bar{k}_1 \hat{r}) \exp(i(\omega_1 t + \phi_1)) + C.C. \quad (3.38)$$

$$E_2 = \frac{E_0}{2} \exp(-i\bar{k}_2 \hat{r}) \exp(i(\omega_2 t + \phi_2)) + C.C., \quad (3.39)$$

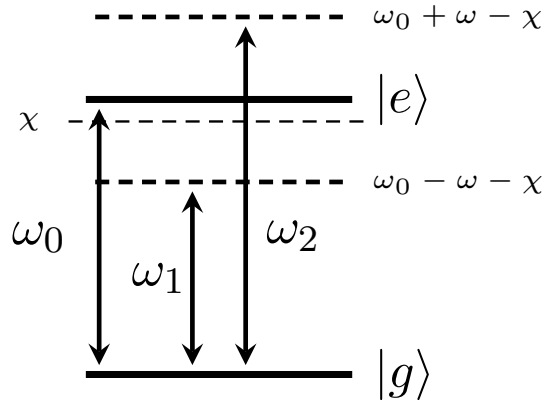


Figure 3.3: The two-level system under investigation.

where  $E_0$  is the amplitude of the field,  $C.C.$  is the complex conjugate,  $\bar{k}$  is the wave vector and  $\phi$  the phase of each field.  $\hat{r}$  is the position of the ion, which oscillates around an equilibrium position  $r_0$  with the small displacement  $\delta\hat{r}$ . The equilibrium term only contributes with a phase factor  $\phi_r$ , but the displacement  $\delta\hat{r}$  (assumed to be in the  $x$ -direction) can in the formalism of annihilation and creation operators [14] be given as

$$\bar{k}\delta\hat{x} = \sum_l^N k_l \sqrt{\frac{1}{2m\omega_l}} (\hat{a} + \hat{a}^\dagger) = \sum_l^N \eta_l (\hat{a} + \hat{a}^\dagger), \quad (3.40)$$

where  $\eta_l = k_l \sqrt{1/2m\omega_l}$  is the Lamb-Dicke parameter. It is from here on assumed that there exists one privileged radiation mode and all other modes are neglected ( $\eta = \sum_l^N k_l \sqrt{1/2m\omega_l} \approx k \sqrt{1/2m\omega}$ ). The Lamb-Dicke parameter is a measure of the ratio between the recoil energy of the ion due to photon emission and the energy separation of the motional states ( $\eta = \sqrt{E_{\text{rec}}/\omega_0}$ ) and it can be interpreted as a measure of the ability of excitation and emission events to change the motional state of the ion. If one assumes the two lasers have the same phase, the total phase can be given as  $\Phi = \phi + r_0$ . If one adds the pieces from equations (3.37, 3.40) one obtains the Hamiltonian given by

$$\hat{H}_I = \left[ \mathcal{D}_1^- \frac{E_0}{2} e^{i\omega_1 t} e^{-i\eta_1(\hat{a} + \hat{a}^\dagger)} e^{i\Phi_1} + \mathcal{D}_2^- \frac{E_0}{2} e^{i\omega_2 t} e^{-i\eta_2(\hat{a} + \hat{a}^\dagger)} e^{i\Phi_2} \right] |g\rangle\langle e| + H.C., \quad (3.41)$$

where  $H.C.$  is the hermitian conjugate. If one make the substitution  $\Omega_i = \mathcal{D}_i \frac{E_0}{2}$ , where  $\Omega_i$  is the Rabi frequency of the  $i$ 'th laser and omits the phase

into the  $\hat{\sigma}_-$ -term and go into the interaction picture with respect to laser  $i$ , one obtains

$$\hat{H}_I = \hat{\sigma}_- \left[ \Omega_1 e^{i\omega_1 t} e^{-i\eta_1(\hat{a} + \hat{a}^\dagger)} + \Omega_2 e^{i\omega_2 t} e^{-i\eta_2(\hat{a} + \hat{a}^\dagger)} \right] + H.C. \quad (3.42)$$

### The Lamb-Dicke Regime

The Lamb-Dicke regime is defined as the limit where the spread of the motional wave function is much less than the wavelength of the light ( $\langle n|r^2|n\rangle \ll 1/k$ ) which is satisfied when  $\eta\sqrt{2n+1} \ll 1$ . The interaction Hamiltonian can in this limit be written as [21]

$$\hat{H}_{\text{LD}} = \Omega_1 \hat{\sigma}_- (1 + i\eta (\hat{a}^\dagger e^{i\omega_1 t} + \hat{a} e^{-i\omega_1 t})) e^{i\phi} + H.C. \quad (3.43)$$

$$+ \Omega_2 \hat{\sigma}_- (1 + i\eta (\hat{a}^\dagger e^{i\omega_2 t} + \hat{a} e^{-i\omega_2 t})) e^{i\phi} + H.C. \quad (3.44)$$

For sufficiently small strength of the laser ( $\Omega \ll \omega_i$ ) and the Rabi frequencies  $\Omega_1 = \Omega/2$  and  $\Omega_2 = \Omega_1 + \epsilon\Omega_1 = (1 + 2\epsilon)\Omega/2$  tuned to the red and blue sideband respectively, the expression can be simplified to

$$\hat{H}_{\text{LD}} = \frac{V}{2\sqrt{N}} (\hat{\sigma}_-(1 + \epsilon)\hat{a}^\dagger - \hat{\sigma}_+(1 + \epsilon)\hat{a}), \quad (3.45)$$

where  $V = \eta\Omega\sqrt{N}$ .

### 3.4.3 Summary

If one adds the terms from the above given derivation one obtains the Hamiltonian:

$$\hat{H} = \frac{\omega_0}{2} \sum_{j=1}^N \hat{\sigma}_{z,j} + \omega \hat{a}^\dagger \hat{a} + \frac{V}{2\sqrt{N}} \sum_{j=1}^N [\hat{\sigma}_{+,j} ((1 + \epsilon)\hat{a} + \hat{a}^\dagger) + \hat{\sigma}_{-,j} ((1 + \epsilon)\hat{a}^\dagger + \hat{a})], \quad (3.46)$$

which will be used in the following chapters.

# Chapter 4

## Standard Dicke Model

This chapter focusses on phases and phase transitions in the standard Dicke model. Initially the mean field equations of motion will be deduced and different approaches to solve these equations will be presented. This will be followed by a section with phase diagrams which also illustrates some of the differences between the different phases and what happens at the phase boundary. The final part of this chapter will describe the fluctuations of the system and analyze the stability of the solutions found by the mean field approach.

### 4.1 Equations of motion for the mean field

In physics and probability theory, mean field theory is a way to treat large and complex models by studying a simpler model. Instead of treating with the complex many-particle model the system is simplified to a one-body model without interacting particles. It is possible to see the mean field approach as the zeroth order expansion of the Hamiltonian in fluctuations. If one seeks further information on the system fluctuations can be added as a perturbation to the mean field description [19].

The time evolution of the system can be described by the master equation approach (see equation (3.26)) and the time evolution of the expectation value of the collective angular momentum operators is hence given by

$$\frac{d}{dt}\langle J_x \rangle = \frac{d}{dt}\text{Tr}(J_x \hat{\rho}(t)) \quad (4.1)$$

$$= \text{Tr}\left(J_x \frac{\partial \hat{\rho}}{\partial t}\right) \quad (4.2)$$

$$= \text{Tr}\left(-iJ_x [\hat{H}, \hat{\rho}] - \frac{J_x}{2} \sum_k \hat{c}_k^\dagger \hat{c}_k \hat{\rho} + \hat{\rho} \hat{c}_k^\dagger \hat{c}_k - 2\hat{c}_k^\dagger \hat{\rho} \hat{c}_k\right) \quad (4.3)$$

$$= \text{Tr}\left(i[\hat{H}, J_x] - \frac{1}{2} \sum_k J_x \hat{c}_k^\dagger \hat{c}_k + \hat{c}_k^\dagger \hat{c}_k J_x - 2\hat{c}_k J_x \hat{c}_k^\dagger\right) \quad (4.4)$$

As long as one only investigates the expectation values one can neglect the noise operators and the time evolution of expectation value of the operators are hence given by:

$$\frac{d\langle \hat{x} \rangle}{dt} = i\langle [\hat{H}, \hat{x}] \rangle + \langle \mathcal{L}(\hat{x}) \rangle, \quad (4.5)$$

where  $\hbar = 1$ ,  $\hat{x}$  is the observable under study, the Hamiltonian,  $\hat{H}$ , is given in equation (3.46) and the Liouvillian operator  $\mathcal{L}(\hat{x})$  can be expressed in the Heisenberg picture in which case it takes the form

$$\mathcal{L}(\hat{x}) = -\sum_k \frac{\gamma_k}{2} \left( \hat{c}_k^\dagger \hat{c}_k \hat{x} + \hat{x} \hat{c}_k^\dagger \hat{c}_k - 2\hat{c}_k \hat{x} \hat{c}_k^\dagger \right) \quad (4.6)$$

If one uses the collective angular momentum operators  $J_i$ ,  $A$  introduced in section (3.1.6) and investigates how they develop in time one can use the above approach. With  $\hat{c}_k = \hat{\sigma}_-$  and  $\gamma_k = \gamma$  one obtains the following for the operator  $J_x$ , where all terms of  $\langle XY \rangle$  is factorized to  $\langle X \rangle \langle Y \rangle$ , where  $X, Y = J_i, A$  for  $i = x, y, z$ :

$$\begin{aligned} \dot{J}_x &= \left\langle \sum_{j=1}^N \dot{\sigma}_{x,j} \right\rangle = i \left\langle \left[ H, \sum_{j=1}^N \hat{\sigma}_{x,j} \right] \right\rangle \\ &\quad + \left\langle \sum_{j=1}^N \frac{\gamma}{2} [2\hat{\sigma}_{+,j} \hat{\sigma}_{x,j} \hat{\sigma}_{-,j} - \hat{\sigma}_{+,j} \hat{\sigma}_{-,j} \hat{\sigma}_{x,j} - \hat{\sigma}_{x,j} \hat{\sigma}_{+,j} \hat{\sigma}_{-,j}] \right\rangle \end{aligned} \quad (4.7)$$

$$= -\frac{\omega_0}{2} J_y + \frac{iV\epsilon}{2\sqrt{N}} J_z (A - A^*) - \frac{\gamma}{2} J_x \quad (4.8)$$

and analogously for  $J_y, J_z$  and  $A$  (the derivation can be found in appendix (A)):

$$\dot{A} = -\frac{iV}{2\sqrt{N}} ((2 + \epsilon)J_x - i\epsilon J_y) - i\omega A \quad (4.9)$$

$$\dot{J}_x = -\frac{\omega_0}{2}J_y + \frac{iV\epsilon}{2\sqrt{N}}J_z(A - A^*) - \frac{\gamma}{2}J_x \quad (4.10)$$

$$\dot{J}_y = \frac{\omega_0}{2}J_x - \frac{V}{2\sqrt{N}}J_z(2 + \epsilon)(A + A^*) - \frac{\gamma}{2}J_y \quad (4.11)$$

$$\dot{J}_z = \frac{V}{2\sqrt{N}}J_y(2 + \epsilon)(A + A^*) - \frac{iV\epsilon}{2\sqrt{N}}J_x(A - A^*) - \gamma\left(J_z + \frac{N}{2}\right) \quad (4.12)$$

### 4.1.1 Steady state solutions

This thesis solves steady state solutions of the above given equations in different ways. One of them is for  $\epsilon = 0$  with the symbolic solve function in matlab and for  $\epsilon \neq 0$  with the numerical fsolve function in matlab. The other is by iteration with matlab's ode45 program. The steady state solutions can mathematically be expressed as

$$\dot{J}_i = 0, \quad \text{where } i = \{x, y, z\} \quad \text{and} \quad (4.13)$$

$$\dot{A} = 0. \quad (4.14)$$

It is advantageous to investigate the steady state solution of a physical experiment which has to be realized experimentally because the experimentalists then don't have to be careful about the timing of their observations. As long as the system is in its steady state it doesn't change and the observer get the same result independent of the time of the measurement. This analysis will hence look into these steady state solutions and describe the behaviour of the system by steady state solutions of the mean field equations given above. For a given state there might be several solutions and different initial conditions will change the state the system ends up in. In later section these differences will be described along with whether all (or none) of these solutions are stable.

The previous mentioned solve approach finds *all* the steady state solutions for given parameters. The fsolve approach finds *one* solution given a set of initial conditions. The ode45 program iterates the time evolution of the coupled differential equation given a set of initial conditions as the fsolve approach. In figure (4.1(a)+4.1(b)) examples of the time evolution simulated

by ode45 is shown, where the system ends in the steady state for the superradiant and normal phase. The value of the collective angular momentum operators are then saved as a function of the parameters. In later sections phase diagrams will be shown where each point is found by this procedure.

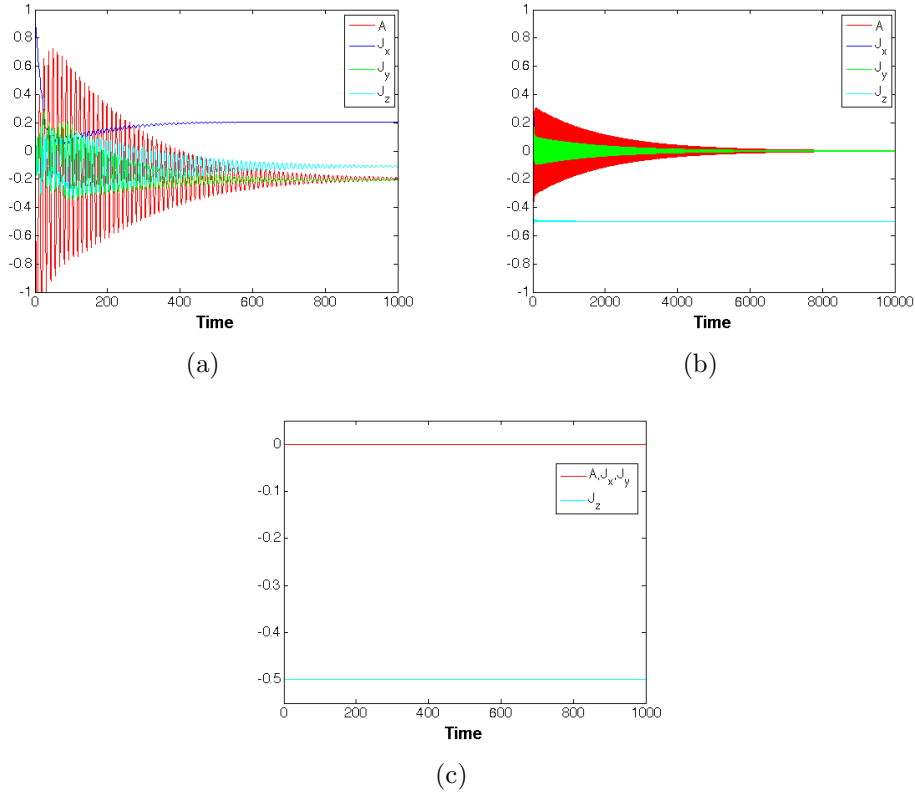


Figure 4.1: Parameters:  $\epsilon = 0.0, \omega = 0.5, \omega_0 = 0.1, \Omega = 0.0, \gamma = 0.1$ . Left: Superradiant phase ( $V = 0.48$ ). Right: Normal phase ( $V = 0.16$ ). It is also seen that for the normal phase is close to the phase transition and hence takes longer to dampen. The one below is with  $J_z = -0.5$  as initial condition.

The four equations of motion (equation (4.9-4.12)) contain three different mean field descriptions of the collective angular momentum operators ( $J_x$ ,  $J_y$  and  $J_z$ ) and the mean field description of the oscillator operator  $A$ . It is possible to reduce these equations to one equation and eliminate three of the variables. It is here chosen to reduce the four equations to one equation with respect to  $J_z$ . In appendix (B) it is possible to see the elimination of the other variables and the result is given in equation (4.15).

$$\begin{aligned}
0 = & - \left( J_z + \frac{1}{2} \right) [2\gamma\delta^2 J_z^4 + 4\beta\delta\gamma J_z^3 + 2\gamma\alpha^2] \\
& - \left( J_z + \frac{1}{2} \right) [4\gamma\alpha\beta J_z + 4\gamma\alpha\delta J_z^2 + 2\gamma\beta^2 J_z^2]
\end{aligned} \tag{4.15}$$

where

$$\alpha = \omega [\omega_0^2 + \gamma^2], \quad \beta = V^2\omega_0 [\epsilon^2 + (2 + \epsilon)^2] / N, \quad \delta = (2 + \epsilon)^2 V^4 \epsilon^2 / \omega N^2 \tag{4.16}$$

It follows that  $J_z = -N/2$  and (see appendix (B))  $A = J_x = J_y = 0$  is a solution and we are left with a fourth order polynomial for the other eventual solutions. Each solution here corresponds to a phase and the case where all ions point down in the  $J_z$  direction is hence one phase.

### 4.1.2 $J_z$ -polynomials

Equation (4.15) is a polynomial with respect to  $J_z$  where the null points indicates a phase. The number of null points are hence the number of phases for the specific setting of parameters. For the different phases a different number of solutions occur as seen in later sections. A way to visualize how these new phases occur is by plotting the  $J_z$ -polynomial for different parameter values. In figure (4.2) three lines are shown each with the same parameters except they have different values of  $V$ 's. The red line only crosses zero once and have hence only one phase, where the green and magenta have the same value of  $J_z$  for one of their phases, but comes up and "touches" the  $x$ -axis. This point is analogous to case where the discriminant in the quadratic equation equals zero and is hence a double-degenerate solution. This will be further analyzed in section (4.2.4). A way to remove this degeneracy is to include a small  $\Omega\hat{\sigma}_x$ , see the inset in figure (4.3). Here it is also seen that the value of  $J_z$  around  $-N/2$  no longer is the same for the different lines. In order for the difference to be substantial a quite large  $\Omega$  is required (here one tenth of the energy differences of the levels in the ion ( $\omega_0$ )). The introduction of this term will be discussed in chapter (5).

The time evolution shown in figures (4.1(a)+4.1(b)) shows how the system ends with  $J_z$ -values that corresponds to the one given below. In the normal phase the value is the same as the  $J_z$ -value where the red line crosses zero. In the superradiant phase it has the  $J_z$ -value of the second null point (this is

the stable solutions, which will be discussed more thoroughly later). IN FIGURE (4.1(c)) it is shown how the system stay in  $J_z = -N/2$  if it starts there even though it is not a stable solution, both for  $V/\sqrt{J} = 0.16$ ,  $V/\sqrt{J} = 0.48$ .

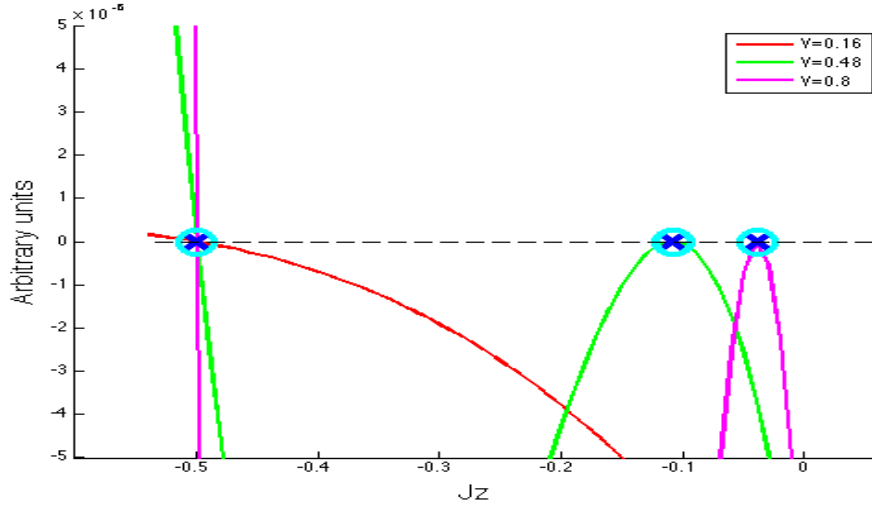


Figure 4.2: Parameters:  $\gamma = 0.1, \epsilon = 0.0, \omega = 0.5, \omega_0 = 0.1, \Omega = 0.0$ . Cyan circle is solutions from *fsolve* and blue crosses solutions from *solve*.

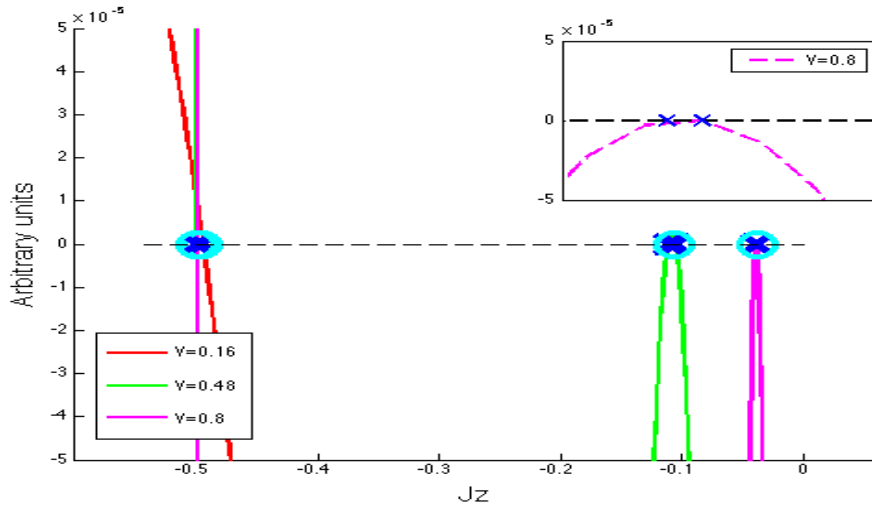


Figure 4.3: Parameters:  $\gamma = 0.1, \epsilon = 0.0, \omega = 0.5, \omega_0 = 0.1, \Omega = 0.01$ . Blue crosses solutions from *solve*. It didn't help with  $\epsilon \neq 0$  and *fsolve*.

### 4.1.3 Phase boundary

In this section an analytical expression for the position of the phase transition is given, both with and without the sideband cooling parameter  $\epsilon$ . The equations of motion given in equation (4.9-4.12) can for  $J_y \neq 0$  through elimination be written as:

$$0 = \omega_0^2 + \gamma^2 + \left( \frac{V^2 (\epsilon^2 + (2 + \epsilon)^2) \omega_0}{N\omega} \right) J_z + \left( \frac{V^4 \epsilon^2 (2 + \epsilon)^2}{N^2 \omega^2} \right) J_z^2 \quad (4.17)$$

from which it follows

$$J_z = - \frac{(NV^2 (\epsilon^2 + (2 + \epsilon)^2) \omega_0 \omega)}{2V^4 \epsilon^2 (2 + \epsilon)^2} \pm \frac{\sqrt{(NV^2 (\epsilon^2 + (2 + \epsilon)^2) \omega_0 \omega)^2 - 4(\omega_0^2 + \gamma^2) (N^2 V^4 \epsilon^2 (2 + \epsilon)^2 \omega^2)}}{2V^4 \epsilon^2 (2 + \epsilon)^2} \quad (4.18)$$

and for  $J_y = 0$ , the  $J_z$ -value must be  $J_z = -N/2$ , which give a phase transition when

$$\frac{N}{2} = \frac{(NV^2 (\epsilon^2 + (2 + \epsilon)^2) \omega_0 \omega)}{2V^4 \epsilon^2 (2 + \epsilon)^2} \pm \frac{\sqrt{(NV^2 (\epsilon^2 + (2 + \epsilon)^2) \omega_0 \omega)^2 - 4(\omega_0^2 + \gamma^2) (N^2 V^4 \epsilon^2 (2 + \epsilon)^2 \omega^2)}}{2V^4 \epsilon^2 (2 + \epsilon)^2} \quad (4.19)$$

or for  $\gamma$ :

$$\gamma = \sqrt{\frac{2V^2(\epsilon^2 + (2 + \epsilon)^2)\omega\omega_0 - V^4\epsilon^2(2 + \epsilon)^2 - 4\omega_0^2\omega^2}{4\omega^2}} \quad (4.20)$$

which goes into equation (4.21) when  $\epsilon = 0$ . The  $\epsilon$  parameter slightly change the position of the phase transition for small  $\epsilon$ , but otherwise doesn't change the conditions for the phase boundary.

$$\gamma = \sqrt{\frac{2V^2\omega_0 - \omega\omega_0^2}{\omega}}. \quad (4.21)$$

In the case with  $\epsilon = 0$  there is only a phase transition for values of  $V$  above a critical  $V$  given by:

$$V \geq V_{\text{critical}} = \sqrt{\frac{\omega\omega_0}{2}}, \quad (4.22)$$

which is consistent with for instance [23, 24]. If one includes  $\epsilon$  the expression gets a bit more cumbersome, but it is possible to show that  $V$  has to be in the interval

$$\sqrt{\frac{2\omega\omega_0}{(2+\epsilon)^2}} \leq V \leq \sqrt{\frac{2\omega\omega_0}{\epsilon^2}}, \quad (4.23)$$

where the lower limit is the same as in equation (4.22) for  $\epsilon = 0$ .

## 4.2 Phase diagrams

The first phase diagram contains a second order phase transition, see figure (4.4). It contains a normal phase (the blue part), where the only nonzero term of the collective angular momentum operators is  $J_z = -0.5$  and a superradiant phase (in the bottom right corner). The phase diagram has been made by iteration of the time evolution with matlab's ode45 program and where each point in the phase diagram is taken as the last value of  $J_z$  from the iteration. An example of how the collective angular momentum operators  $A, J_i$  where  $i \in \{x, y, z\}$  develops according the ode45 is shown in figure (4.1(a)).

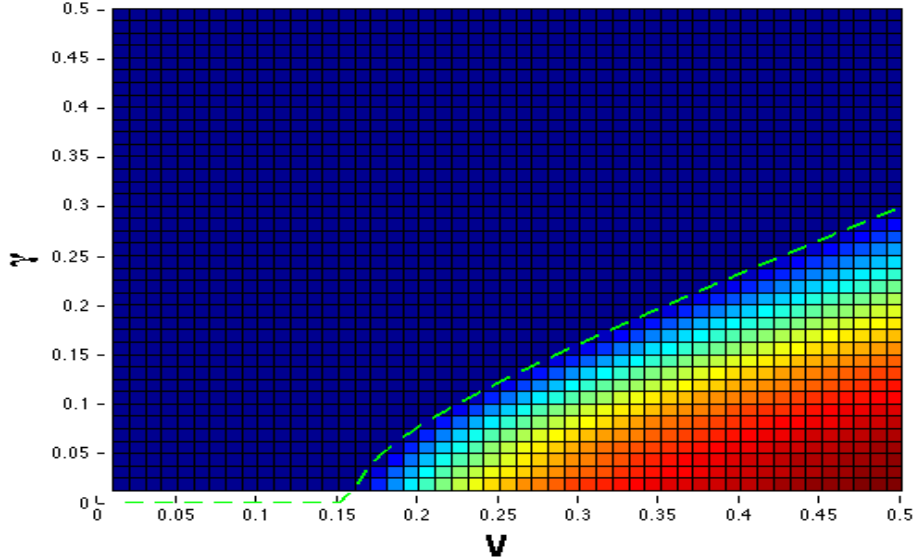


Figure 4.4: This figure shows a second order phase transition with a normal phase (blue) and a superradiant phase (bottom right corner). Parameters used:  $\epsilon = 0.0, \omega = 0.5, \omega_0 = 0.1, \Omega = 0.0$ .

The green dashed line corresponds to the analytical solution of where the phase boundary is, given by equation (4.21) and there is no phase transition for values of  $V$  less than  $V_{\text{critical}} = \sqrt{\omega\omega_0}/2$  as expected by equation (4.22). The approach is hence consistent with the analytical solution. It is also seen in figure (4.4) that it is possible to see a second order phase transition, both if one increase the laser coupling parameter  $V$  or the dissipation  $\gamma$ .

### Consistency between ode45 and fsolve

If one goes to larger  $V$ 's a new phenomena is observed. It is shown in figures (4.5+4.6). The figures have been produced with the matlab programs ode45 and fsolve respectively, where in the last case the value of  $J_z$  was set to zero if no stable solutions were found (what is meant with stable solutions will become clear in section (4.3)). There is observed a consistency between the numerical solution of the steady state equations for the equations of motion and the time evolution from ode45. The phase transition is furthermore found to be consistent with equation (4.21) indicated by the blue (green) dashed line.

The region with many different colors in the ode45 plot and dark red in the fsolve plot is a chaotic phase where there is no stable solutions and this

chaotic behaviour will be left for chapter (6). The phases differs by (a) the time evolution of the collective angular momentum operator (see section (4.2.3)), (b) broken symmetry (see section (4.2.4)) and (c) number of stable solutions (see section (4.3.4)).

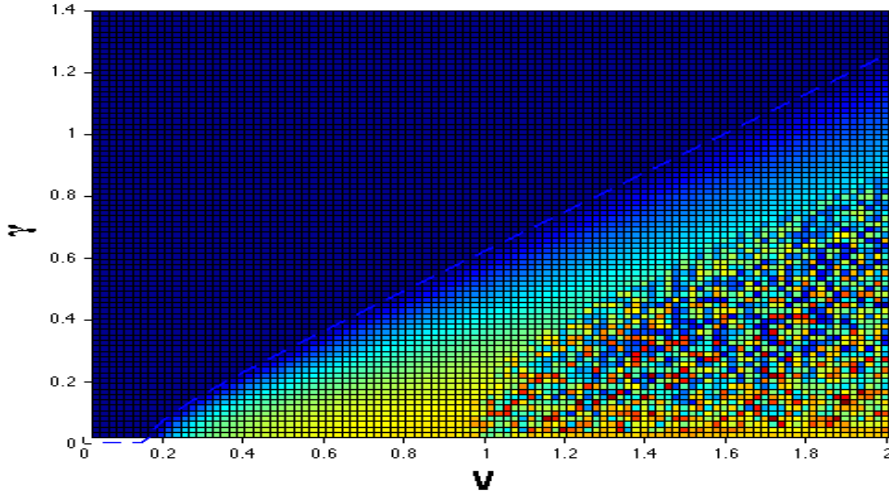


Figure 4.5: Parameters:  $\epsilon = 0.0, \omega = 0.5, \omega_0 = 0.1, \Omega = 0.0$ . Red: analytical solution without  $\epsilon$ . Blue with  $\epsilon$ . Both without  $\Omega$ . ode45

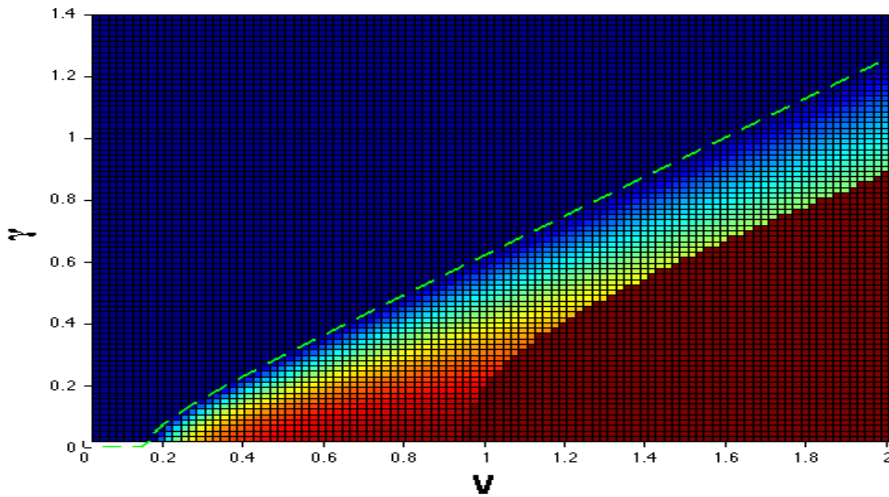


Figure 4.6: Parameters:  $\epsilon = 0.0, \omega = 0.5, \omega_0 = 0.1, \Omega = 0.0$ . fsolve where  $J_z = 0$  if no stable solutions (stability will be discussed more thoroughly later).

### 4.2.1 $\epsilon$ changes the phase diagram for larger $V$ 's

If one includes the sideband cooling parameter  $\epsilon$  the phase diagram changes. The idea behind the inclusion is to reduce the fluctuations, which will be shown in section (4.3.3). In section (4.1.3) expressions for  $\gamma(V)$  was shown (see equations (4.20+4.21)). Beside this expression for the phase boundary also critical values of  $V$  was shown, see equations (4.22+4.23).

It is seen in figures (4.7+4.8) that for  $V < 2$  the inclusion of  $\epsilon$  only changes the phase boundary slightly, whereas for larger  $V$ 's it becomes crucial. For values of  $V$  larger than  $\sqrt{2\omega\omega_0/\epsilon^2}$  only the normal phase exist when  $\epsilon \neq 0$  as in the case for  $V \leq \sqrt{2\omega\omega_0/(2+\epsilon)^2}$  as expected by equation (4.23). A new region is also seen in figure (4.7) for larger values of  $V$  in the case  $\epsilon = 0$ . This region will be treated in section (??).

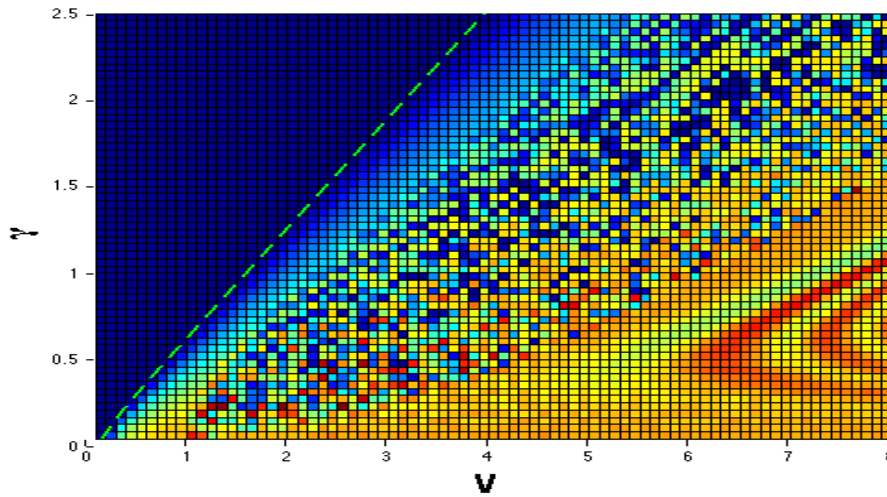


Figure 4.7: Parameters:  $\epsilon = 0.0, \omega = 0.5, \omega_0 = 0.1, \Omega = 0.0$ . Red: analytical solution without  $\epsilon$ . Blue with  $\epsilon$ . Both without  $\Omega$ . .. the upper bound for  $V$  is observed consistent with equation (4.23)

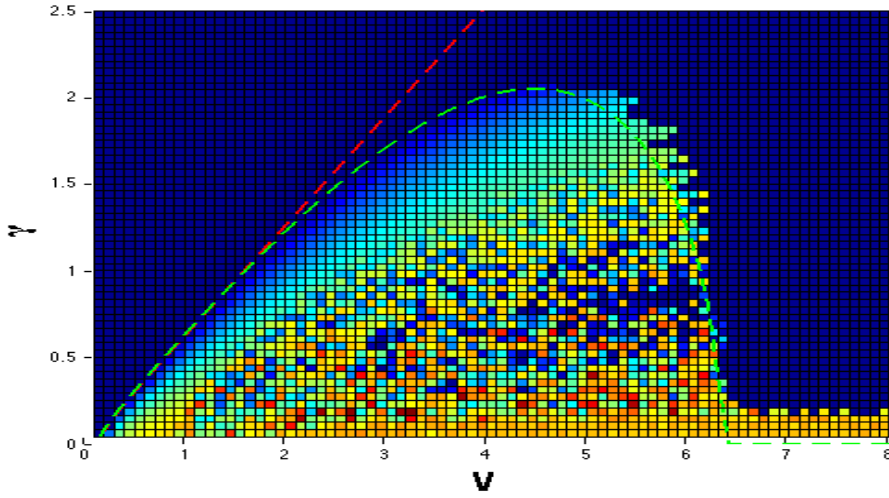


Figure 4.8: Parameters:  $\epsilon = 0.05, \omega = 0.5, \omega_0 = 0.1, \Omega = 0.0$ . Red: analytical solution without  $\epsilon$ . Blue with  $\epsilon$ . Both without  $\Omega$ . .. the upper bound for  $V$  is observed consistent with equation (4.23)

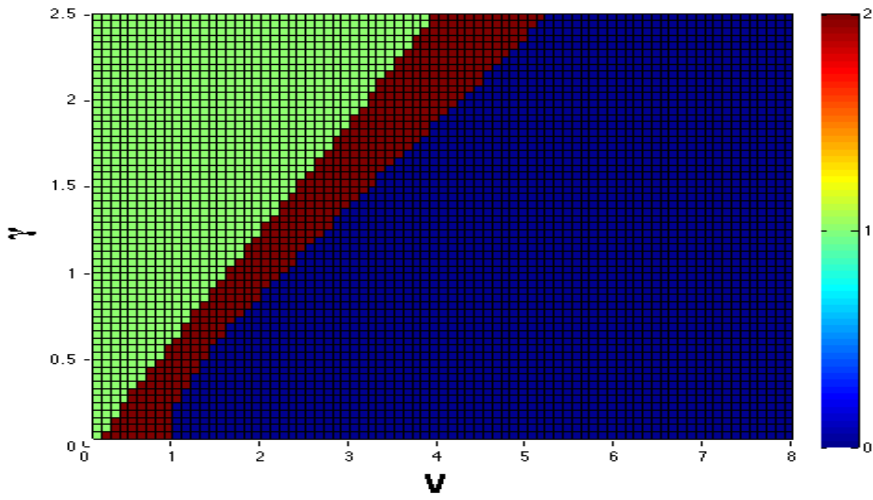


Figure 4.9: Parameters:  $\epsilon = 0.05, \omega = 0.5, \omega_0 = 0.1, \Omega = 0.0$ . Red: analytical solution without  $\epsilon$ . Blue with  $\epsilon$ . Both without  $\Omega$ . .. the upper bound for  $V$  is observed consistent with equation (4.23)

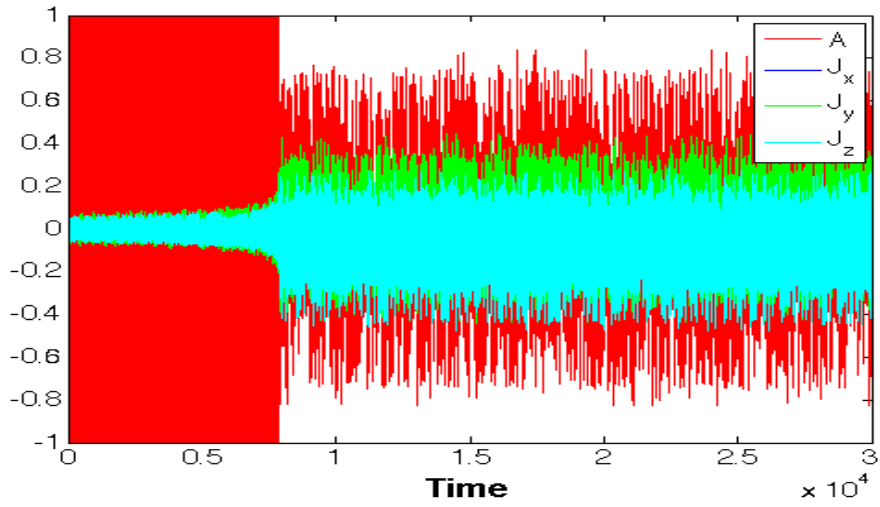


Figure 4.10: Parameters:  $\epsilon = 0.0, \omega = 0.5, \omega_0 = 0.1, \Omega = 0.0, \gamma = 0.5, V = 7.0$ . This figure shows the time evolution in one of the points in the new phase. It is not stable and keeps oscillating also for larger time scales.

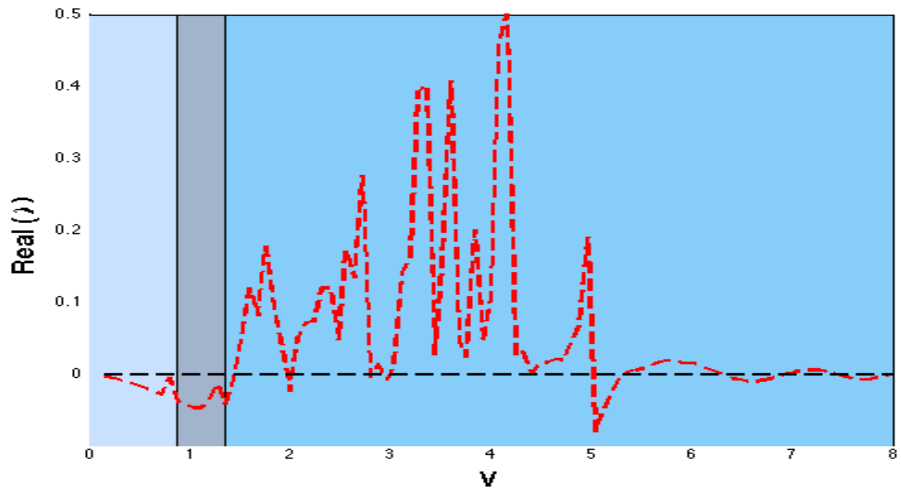


Figure 4.11: Parameters:  $\epsilon = 0.0, \omega = 0.5, \omega_0 = 0.1, \Omega = 0.0, \gamma = 0.5$ . The largest real part of the eigenvalues of the fluctuations.

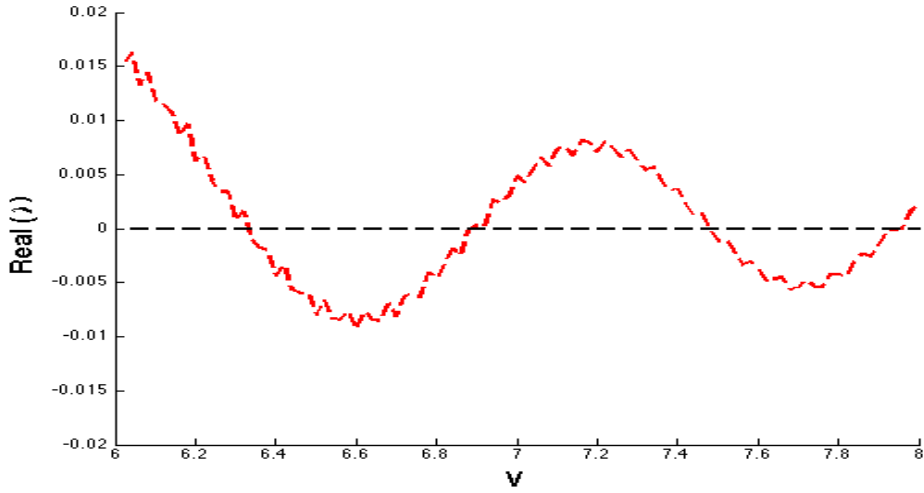


Figure 4.12: Parameters:  $\epsilon = 0.0, \omega = 0.5, \omega_0 = 0.1, \Omega = 0.0, \gamma = 0.5$ . The largest real part of the eigenvalues of the fluctuations.

#### 4.2.2 The phase diagram is time independent

In section (4.1.1) steady state solutions were explained and assume the system to end in a steady state. In the normal and superradiant phase it is also seen that the systems develops according the ode45 into a stable state which is equal to the solution of the steady state equations. It is not clear whether this is also the case for the chaotic phase, where no stable solutions occur and according to the  $J_z(t)$ -graphs the values changes for each new iteration. Figures (4.14+4.13) show that this behaviour is constant in time and that it hence not simply is a question of too short a timescale. So where the values of  $J_z$  depends on the time in the chaotic phase the overall phase diagram is the same.

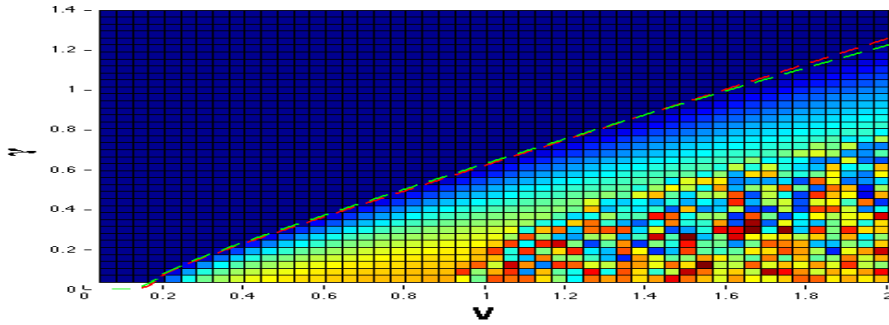


Figure 4.13: Parameters:  $\epsilon = 0.05, \omega = 0.5, \omega_0 = 0.1, \Omega = 0.0$ . Red: analytical solution without  $\epsilon$ . Blue with  $\epsilon$ . Both without  $\Omega$ . Number of iterations (ode45): 5,000.

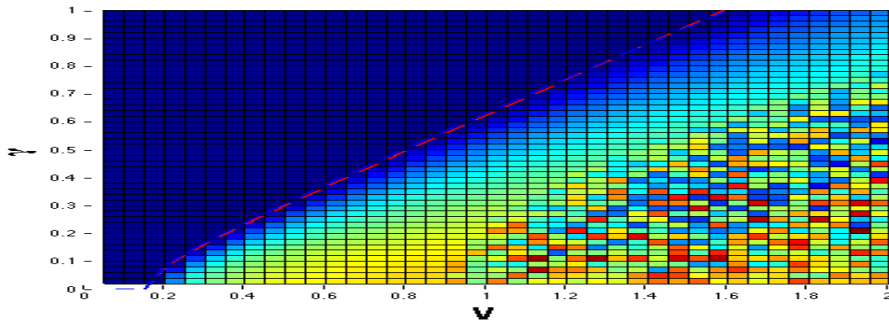


Figure 4.14: Parameters:  $\epsilon = 0.05, \omega = 0.5, \omega_0 = 0.1, \Omega = 0.0$ . Red: analytical solution without  $\epsilon$ . Blue with  $\epsilon$ . Both without  $\Omega$ . Number of iterations (ode45): 10,000.

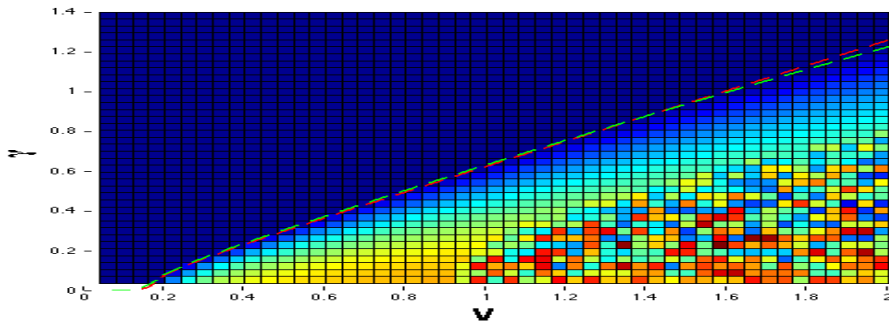


Figure 4.15: Parameters:  $\epsilon = 0.05, \omega = 0.5, \omega_0 = 0.1, \Omega = 0.0$ . Red: analytical solution without  $\epsilon$ . Blue with  $\epsilon$ . Both without  $\Omega$ . Number of iterations (ode45): 20,000.

### 4.2.3 $J_z(t)$ -graphs

In figures (4.16-4.19) the time evolution of  $A$  and  $J_i$  is shown in the normal phase (figure 4.16), the super-radiant phase (figure 4.17) and the chaotic phase (figures 4.18+4.19), where the second is a zoom of the last 1000 iterations from the first figure. It is clear that the  $J_z$ -values in the normal phase and superradiant phase origin from a steady state solution, but there is no steady state solution in the chaotic regime and the value taken depends hence on where one chooses to stop the iteration.

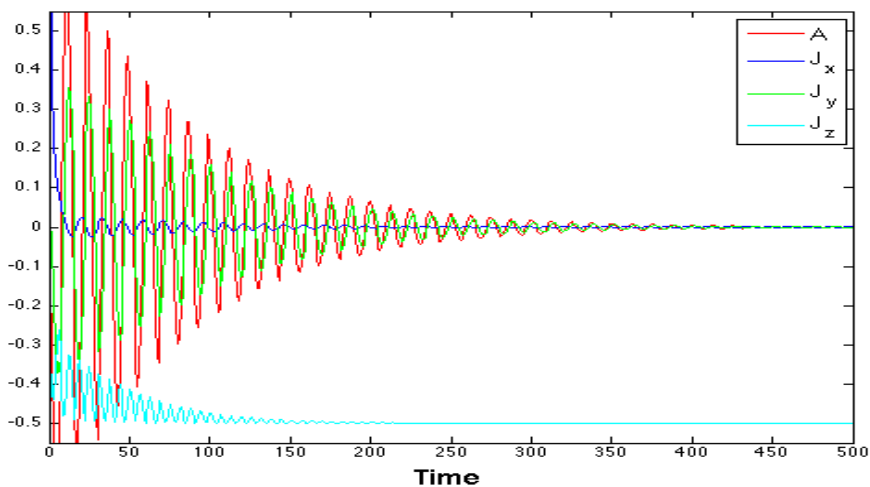


Figure 4.16: Parameters:  $\epsilon = 0.0, \omega = 0.5, \omega_0 = 0.1, \Omega = 0.0, \gamma = 1.0, V = 0.5$ .  
Normal phase

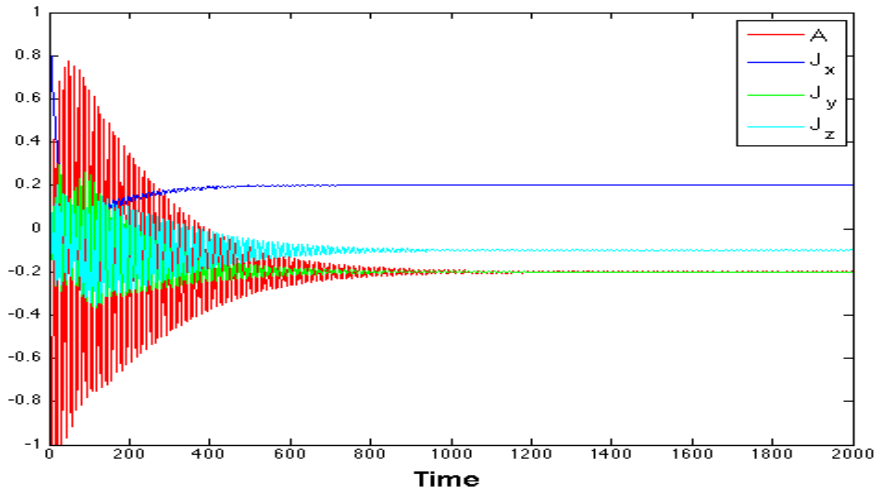


Figure 4.17: Parameters:  $\epsilon = 0.0, \omega = 0.5, \omega_0 = 0.1, \Omega = 0.0, \gamma = 0.1, V = 0.5$ .  
Superradiant phase

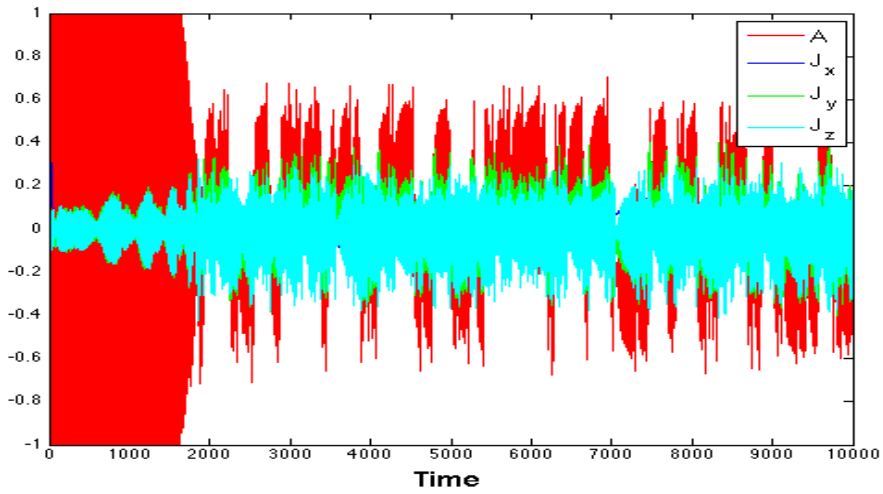


Figure 4.18: Parameters:  $\epsilon = 0.0, \omega = 0.5, \omega_0 = 0.1, \Omega = 0.0, \gamma = 0.1, V = 1.5$ .  
Chaotic phase

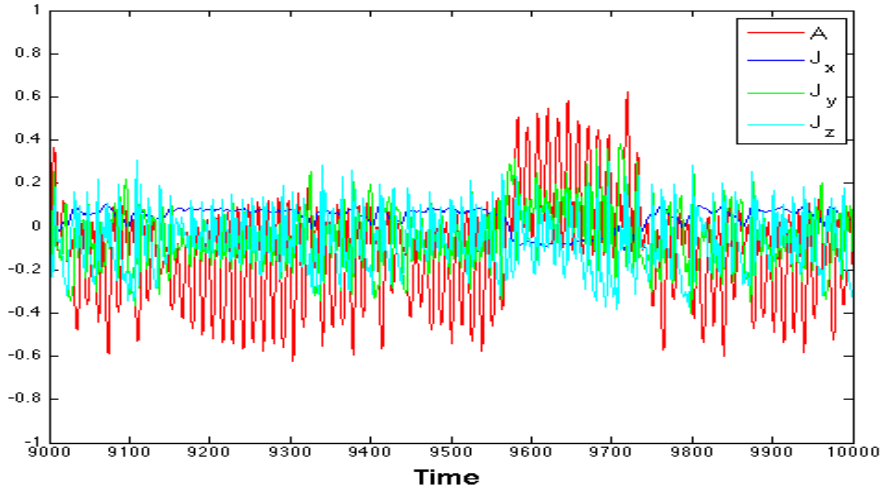


Figure 4.19: Parameters:  $\epsilon = 0.0, \omega = 0.5, \omega_0 = 0.1, \Omega = 0.0, \gamma = 0.1, V = 1.5$ .  
Chaotic phase (zoom)

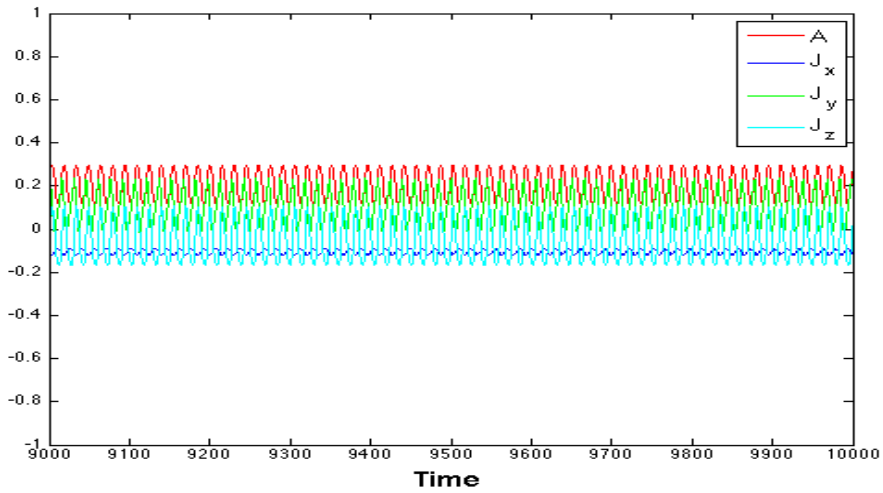


Figure 4.20: Parameters:  $\epsilon = 0.0, \omega = 0.5, \omega_0 = 0.1, \Omega = 0.0, \gamma = 0.1, V = 1.0$ .  
Boundary between chaotic and superradiant phase. At the phase boundary it takes forever for the system to be damped. All this figures with  $J_z(t)$  could be referred to in the phase diagram with a cross on the relevant points.

#### 4.2.4 Broken symmetry

As seen in section (4.1.2) there exists a double degenerate solution in the superradiant and chaotic phase. If one plots the values of  $A, J_x$  or  $J_y$  instead

it is observed that the transition from the normal phase to the superradiant phase breaks their symmetry and where there in the normal phase is *one* solution there is now *three* solutions. Which one the system ends up in depends on the initial conditions, i.e. whether the system starts in  $J_x$ ,  $J_y$  or  $J_z$  state. In figures (4.21-4.23) the values of  $J_x$  is plotted. The background colors illustrates the different phases and it is also seen from the figures that this way to express the states shows no difference between the chaotic and superradiant phase. The difference between these states will was partly seen in section (4.2.3) with the time evolution of the collective angular momentum operators in the different phases and will also be seen in section (4.3.4) with the number of stable solutions.

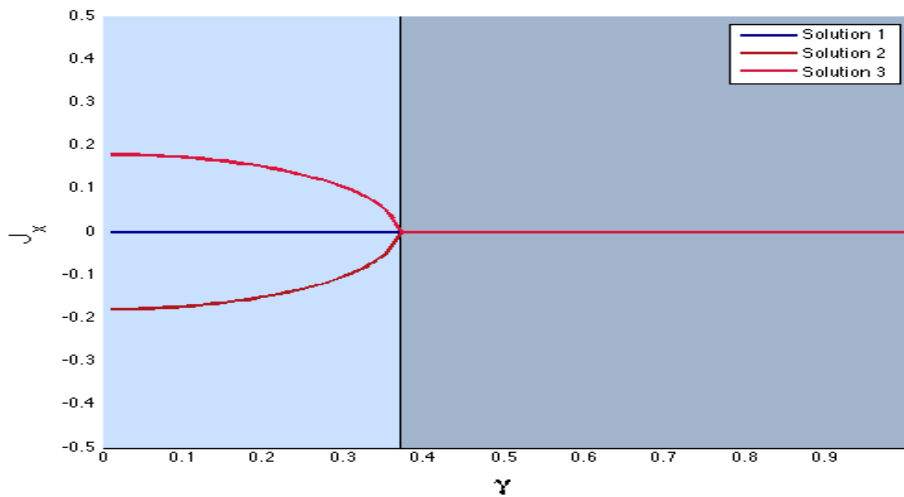


Figure 4.21: The parameters used to produce this figure are:  $\epsilon = 0.0$ ,  $\omega = 0.5$ ,  $\omega_0 = 0.1$ ,  $\Omega = 0.0$ ,  $V = 0.6$ . It shows how the broken symmetry of the superradiant phase transition breaks at the phase boundary when one cranks up the dissipation.

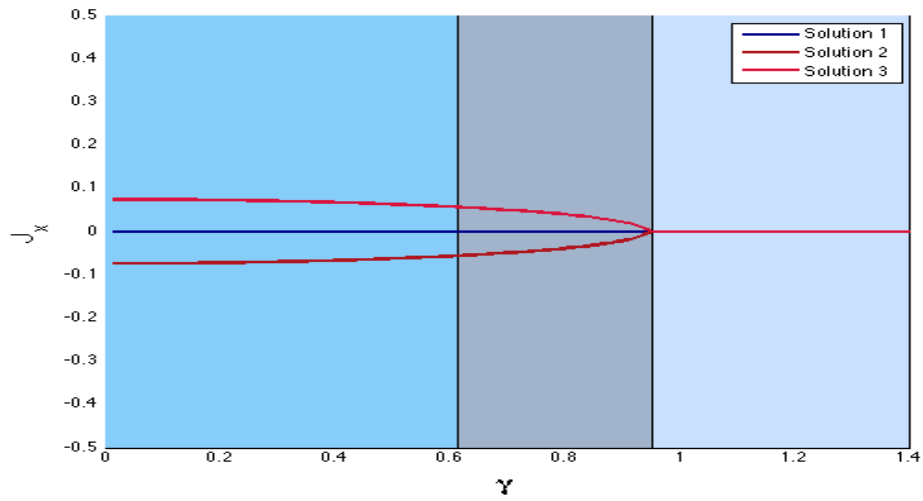


Figure 4.22: The parameters used to produce this figure are:  $\epsilon = 0.0, \omega = 0.5, \omega_0 = 0.1, \Omega = 0.0, V = 1.5$ . It is seen that the phase transition between the normal phase and the superradiant phase breaks the symmetry (also seen in figure (4.21)), but nothing happens when one goes from the superradiant to the chaotic phase.

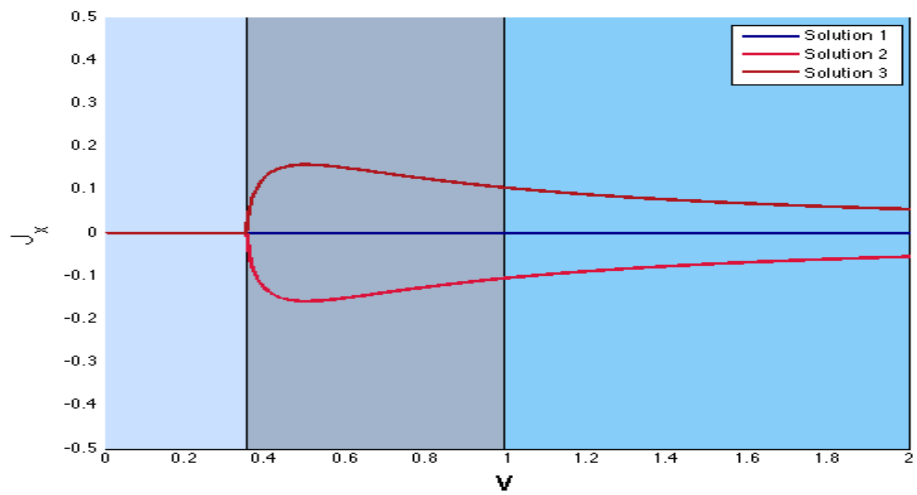


Figure 4.23: The parameters used to produce this figure are:  $\epsilon = 0.0, \omega = 0.5, \omega_0 = 0.1, \Omega = 0.0, \gamma = 0.2$ . This figure shows the same behaviour as figure (4.22) when one scan over  $V$  instead of  $\gamma$ .

## 4.3 Fluctuations and stability of the system

So far only the mean field evolution of the system has been investigated. It has been shown that there exist different phases and in some of these phases several solutions exist. This section will develop a tool which enables one to check the stability of the found solutions and it gives hence a way to characterize the different phases. This section will only include the first order in the expansion of the mean field and a linearization of the noise is hence made.

If a system is in an unstable state, just the smallest perturbations will drag the system away from this state. If the system is stable a small perturbation will not leave the state altered; after a short time it will be back in its equilibrium position given by the mean field equations in this case. Examples of an unstable point in two dimension are a saddlepoint and a knot, where a small perturbation along one (two) axes will take the system away from its equilibrium position.

### 4.3.1 Linearization of the fluctuations

An operator can be written as an expectation value and its fluctuations around it, where one can truncate the larger order of the fluctuations.

$$\hat{O} = O + \delta\hat{O} + \mathcal{O}((\delta O)^2), \quad (4.24)$$

where  $\hat{O}$  is the operator,  $O$  the expectation value and  $\delta\hat{O}$  is the fluctuations. If one take the time derivative of this equation one obtains

$$\frac{d\hat{O}}{dt} = \frac{dO}{dt} + \frac{d\delta\hat{O}}{dt} \quad (4.25)$$

which enables one to get an equation of the time derivative of the fluctuations

$$\frac{d\delta\hat{O}}{dt} = \frac{d\hat{O}}{dt} - \frac{dO}{dt}. \quad (4.26)$$

In the following the noise operators  $\delta\hat{A}$  and  $\delta\hat{J}_i$  will be deduced.

**Example:**  $\delta\hat{A}, \delta\hat{A}^*$ -terms

According to equation (4.24) the  $\hat{A}$ -operator can be expressed as

$$\hat{A} = A + \delta\hat{A} \quad (4.27)$$

and the time derivative of the noise as

$$\frac{d\delta\hat{A}}{dt} = \frac{d\hat{A}}{dt} - \frac{dA}{dt}. \quad (4.28)$$

If one chooses  $\frac{dA}{dt}$  to be

$$\frac{dA}{dt} = -\frac{iV}{2\sqrt{N}} [(2 + \epsilon) J_x - i\epsilon J_y] - i\omega A \quad (4.29)$$

equation (4.28) reduces to

$$\frac{d\delta\hat{A}}{dt} = -\frac{iV}{2\sqrt{N}} [(2 + \epsilon) \delta\hat{J}_x - i\epsilon\delta\hat{J}_y] - i\omega\delta\hat{A} \quad (4.30)$$

and  $\frac{d\delta\hat{A}^*}{dt}$  is hence given by

$$\frac{d\delta\hat{A}^*}{dt} = \frac{iV}{2\sqrt{N}} [(2 + \epsilon) \delta\hat{J}_x + i\epsilon\delta\hat{J}_y] + i\omega\delta\hat{A}^*. \quad (4.31)$$

The time evolution of the fluctuations for the  $\hat{J}_i$  terms is found analogously and given in section (4.3.1)

### **Time derivative of the fluctuations**

The time derivative of the fluctuations around the mean values are given in the equations below.

$$\frac{d\delta\hat{A}}{dt} = -\frac{iV}{2\sqrt{N}} \left[ (2 + \epsilon) \delta\hat{J}_x - i\epsilon\delta\hat{J}_y \right] - i\omega\delta\hat{A} \quad (4.32)$$

$$\frac{d\delta\hat{A}^*}{dt} = \frac{iV}{2\sqrt{N}} \left[ (2 + \epsilon) \delta\hat{J}_x + i\epsilon\delta\hat{J}_y \right] + i\omega\delta\hat{A}^* \quad (4.33)$$

$$\frac{d\delta\hat{J}_x}{dt} = -\frac{\omega_0}{2}\delta\hat{J}_y + \frac{iV\epsilon}{2\sqrt{N}}\delta\hat{J}_z(A - A^*) + \frac{iV\epsilon}{2\sqrt{N}}J_z(\delta\hat{A} - \delta\hat{A}^*) - \frac{\gamma}{2}\delta\hat{J}_x \quad (4.34)$$

$$\begin{aligned} \frac{d\delta\hat{J}_y}{dt} &= \frac{\omega_0}{2}\delta\hat{J}_x - \frac{V}{2\sqrt{N}}\delta\hat{J}_z(2 + \epsilon)(A + A^*) \\ &\quad - \frac{V}{2\sqrt{N}}J_z(2 + \epsilon)(\delta\hat{A} + \delta\hat{A}^*) - \frac{\gamma}{2}\delta\hat{J}_y \end{aligned} \quad (4.35)$$

$$\begin{aligned} \frac{d\delta\hat{J}_z}{dt} &= \frac{V}{2\sqrt{N}}\delta\hat{J}_y(2 + \epsilon)(A + A^*) + \frac{V}{2\sqrt{N}}J_y(2 + \epsilon)(\delta\hat{A} + \delta\hat{A}^*) \\ &\quad - \frac{iV\epsilon}{2\sqrt{N}}\delta\hat{J}_x(A - A^*) - \frac{iV\epsilon}{2\sqrt{N}}J_x(\delta\hat{A} - \delta\hat{A}^*) - \gamma\delta\hat{J}_z. \end{aligned} \quad (4.36)$$

One is left with a set of coupled differential equations where all terms of  $\delta\hat{X} \cdot \delta\hat{X}$ , where  $\hat{X} = \hat{J}_i$  or  $\hat{X} = \hat{A}$ , where  $i \in \{x, y, z\}$  has been truncated. It is hence possible to describe the time evolution of the fluctuation in terms of a matrix, which satisfies

$$\dot{\bar{v}} = \mathbb{M} \cdot \bar{v}, \quad (4.37)$$

where the vector  $\bar{v}$  is given by

$$\bar{v} = (\delta\hat{A} \quad \delta\hat{A}^* \quad \delta\hat{J}_x \quad \delta\hat{J}_y \quad \delta\hat{J}_z)' \quad (4.38)$$

Matlab's eigenvalue function enables one to diagonalize the matrix  $\mathbb{M}$  and obtain the eigenvalues. The eigenvalues give information on the stability of the system and whether or not the system heat up. In later sections different solutions' stability is checked with this procedure and specifically to check whether the system become less heated up by introducing the parameter  $\epsilon$ . It is only the real part of the eigenvalues which are of interest, because positive real values indicates the fluctuations grows exponentially with the time and the system is hence unstable and if the real part of the eigenvalues are negative the system is stable.

### 4.3.2 Results from linearization of the fluctuations

The way to determinate whether a solution is stable or not is by diagonalization of the matrix representing the time evolution of the fluctuations. The largest value of the real part from the eigenvalues are plotted in figure (4.24+4.25). It is seen that the real part of the eigenvalues are below zero in the normal and superradiant phase, which means the solutions are stable. In the chaotic regime some values of the noise are below and some above zero, which indicates regions with stable solutions. The different background colours represent the different phases the system is in. It is also seen that right at the phase boundary between the normal and superradiant phase the real part of the eigenvalues increase and in some cases goes above zero. This indicates that just at the phase boundary the system is in general unstable.

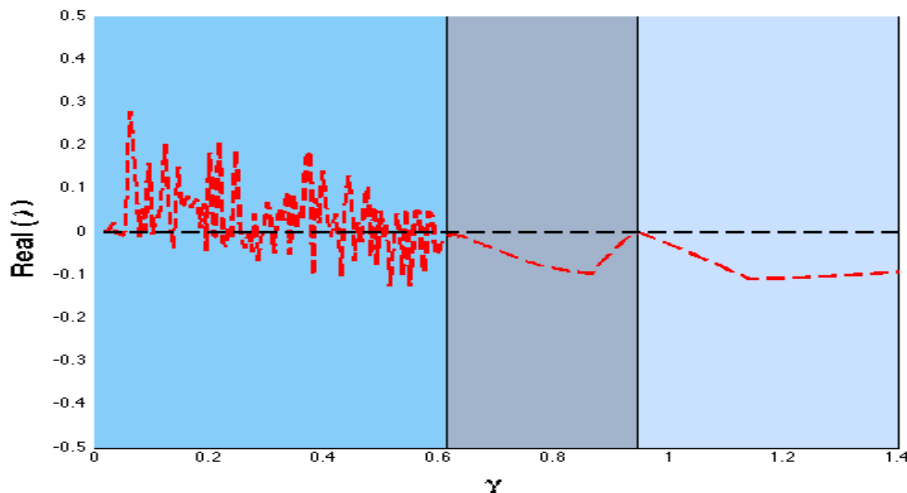


Figure 4.24: This figure shows the largest real part of the eigenvalues from the matrix representing the time evolution of the fluctuations. The background colors represent the chaotic, superradiant and normal phase if one goes from left to right. The parameters used to make this figure is  $\epsilon = 0.0$ ,  $\omega = 0.5$ ,  $\omega_0 = 0.1$ ,  $\Omega = 0.0$ ,  $V = 1.5$ .

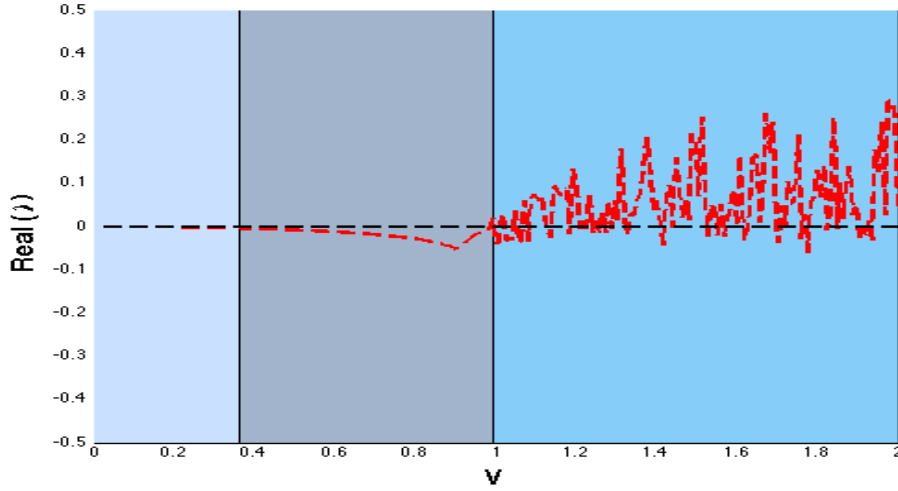


Figure 4.25: This figure shows the largest real part of the eigenvalues from the matrix representing the time evolution of the fluctuations. The background colors represent the normal, superradiant and chaotic phase if one goes from left to right. The parameters used to make this figure is  $\epsilon = 0.0, \omega = 0.5, \omega_0 = 0.1, \Omega = 0.0, \gamma = 0.2$ .

### 4.3.3 Influence of the $\epsilon$ parameter

The system under investigation seems from above given analysis to have stable solutions in the normal and superradiant phase, but if an experimentalist wants to perform this experiment an increased heating cannot be excluded. In order to reduce the heating of the system this thesis has suggested the inclusion of the  $\epsilon$  parameter, which models an inclusion of sideband cooling. In figure (4.26) the largest real part of the eigenvalues of the fluctuations are shown for three different  $\epsilon$  and it is seen that larger  $\epsilon$ 's reduce the fluctuations in the stable phases. An exception for this is on the phase boundary, which in its nature is unstable.

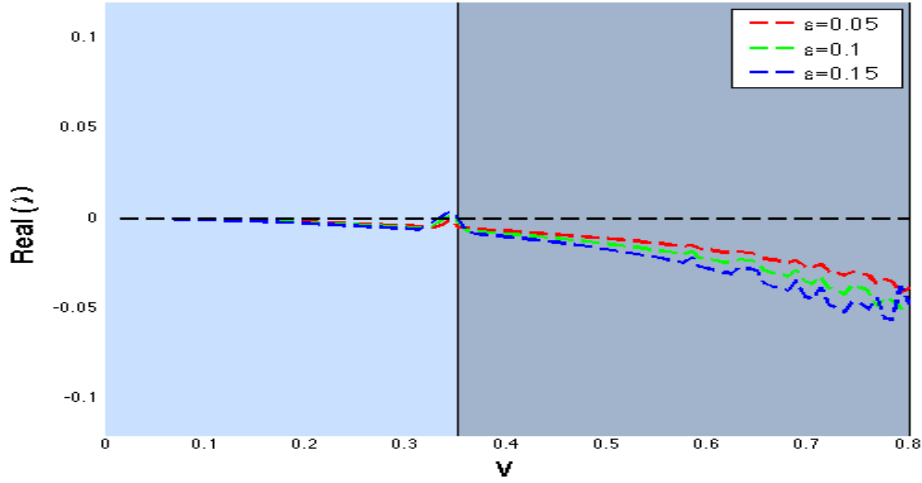


Figure 4.26: Parameters:  $\epsilon = 0.0, \omega = 0.5, \omega_0 = 0.1, \Omega = 0.0, \gamma = 0.2$  .

#### 4.3.4 Number of stable solutions

In figures (4.27 + 4.28) the number of solutions and stable solutions are shown. In the normal phase only one solution occurs with  $J_z$  as the only nonzero entry ( $J_z = -0.5$ ). In the superradiant and chaotic three phases occur of which two are stable in the superradiant phase. This superradiant phase is a double degenerate phase in  $J_z$ , where the other terms have a sign difference as the only difference between the two phases as seen in section (4.2.4) about broken symmetry. This double degeneracy can be lifted by an inclusion of the driving term  $\Omega \hat{\sigma}_x$ , see section (4.1.2) with  $J_z$ -polynomials.

In table (4.1) one point from the phase diagram presented in figure (4.14) is investigated. The first three columns presents the three solutions to the steady state equations, where the second and third are stable in this regime. The fourth and fifth column shows the results from the iterative solution from the ode45-program, where the difference between the two columns is the initial conditions. Column 4 start with  $J_x = 1$  and column 5 with  $J_y = 1$  (the rest are zero). It is observed that dependent on the initial conditions the system evolves into either of the two stable phases. In column 6 a third iterative solution from the ode45-program is shown where the system initially was in the  $J_z = 1$  state. This state is unstable so just the smallest perturbation will force the system to develop into one of the two stable solutions.

In section (4.2.4) it was shown how the phase transition between the nor-

Variable	SSS1	SSS2	SSS3	IS1	IS2	IS3
$A$	0	0.1807	-0.1807	-0.1810	0.1808	0
$J_x$	0	-0.1506	0.1506	0.1505	-0.1506	0
$J_y$	0	0.3011	-0.3011	-0.3009	0.3015	0
$J_z$	-0.5	-0.1736	-0.1736	-0.1746	-0.1725	-0.5

Table 4.1: The columns "SSS" presents the steady state solutions and the columns "IS 1 (2,3)" presents the results from the ode45 solution with 10,000 iterations, where the initial conditions are for (IS 1):  $J_x = 1$ , for (IS 2):  $J_y = 1$  and for (IS 3):  $J_z = 1$  and the other terms equal to zero. The parameter values are  $\gamma = 0.2, V = 0.6, \epsilon = 0.0, \omega = 0.5, \omega_0 = 0.1, \Omega = 0.0$ . REFER TO GREEN CROSS IN SOME PHASE DIAGRAM??

mal and superradiant phase breaks the symmetry of the normal phase and this section shows how at the phase transition between the superradiant and chaotic phase the number of stable solutions decreases from two to zero.

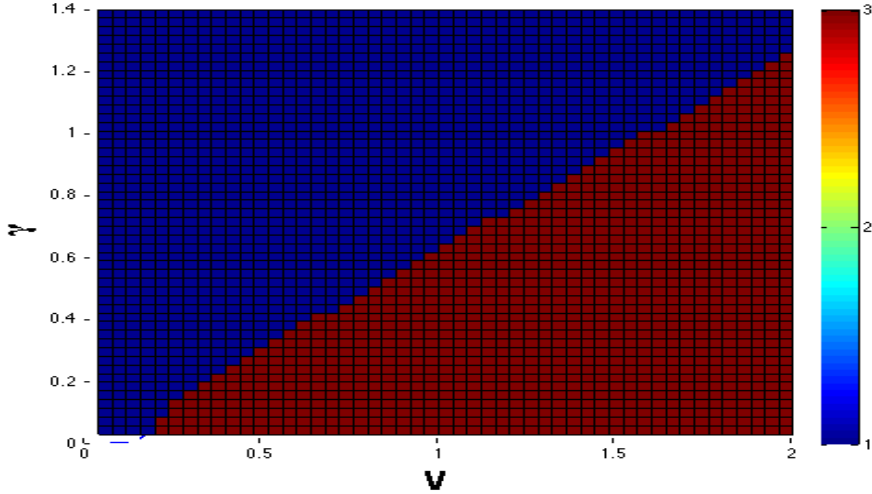


Figure 4.27: This figure shows the number of solutions for different  $V$ 's and  $\gamma$ 's. In the normal phase there is one solution and in the superradiant and chaotic phase three solutions occur. The parameters used to produce this figure is  $\epsilon = 0.0, \omega = 0.5, \omega_0 = 0.1, \Omega = 0.0$ .

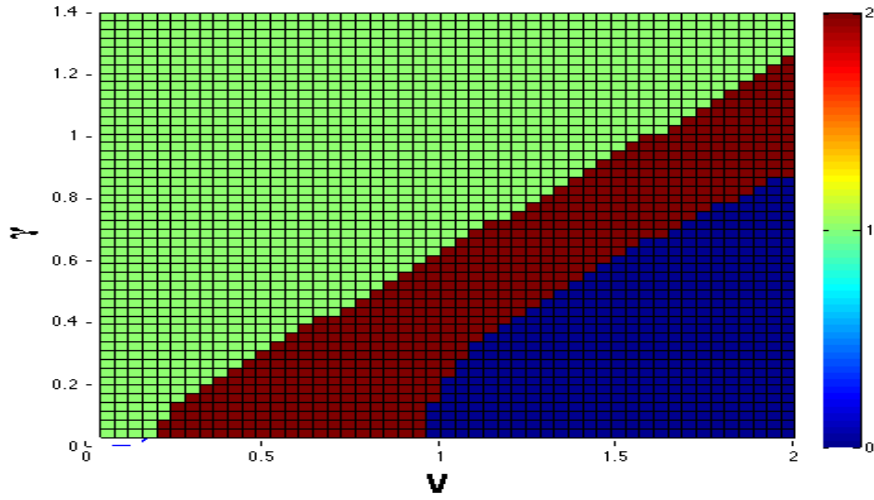


Figure 4.28: This figure shows the number of stable solutions for different  $V$ 's and  $\gamma$ 's. In the normal phase there is one stable solution, in the superradiant phase there is two stable solutions and in the chaotic phase there is none.. The parameters used to produce this figure are  $\epsilon = 0.0, \omega = 0.5, \omega_0 = 0.1, \Omega = 0.0$ .

# Chapter 5

## Extended Dicke model

In the previous chapter the standard Dicke model was investigated with the inclusion of sideband cooling in form of the parameter  $\epsilon$ . Several papers has taken the Dicke model and investigated it in different setup (it could be in optical cavity QED [8], trapped ions [25] or in open systems [10]) and investigated small changes of the above given pure Dicke model (equation (3.29)).

This thesis will also alter the Dicke model to a denoted "extended" Dicke model. The extended Dicke model adds an element to the standard Dicke model. It introduces a new  $\hat{\sigma}_x$ -term to the Hamiltonian. The motivation to do this is to add yet a competing term to the dissipation. It gives rise to new phase transitions and this thesis investigates both this new phase transition and also how the phase transition of the standard model behaves when one cranks up the new  $\hat{\sigma}_x$ -term.

This chapter will initially start with the standard Dicke model with the introduction of a small driving term  $\Omega\hat{\sigma}_x$ . This will be followed by another limit for  $\Omega$  where the ionic term  $\omega_0$  is so small it is neglected in the analysis. This last section will be described in two parts, one with and one without sideband cooling (in form of  $\epsilon$ ). The tools used in previous section will be used again but they will not explained as thoroughly again and all the derivation will in contrast to previous chapter come initially.

### 5.1 Equations of motion

This section will briefly present the equations of motion with the inclusion of the new driving term

$$\hat{H}_{\text{driving}} = \frac{\Omega}{2} \sum_{j=1}^N \hat{\sigma}_x \quad (5.1)$$

which origin from another laser field interacting with the ions. A laser which drive the  $|g\rangle \leftrightarrow |e\rangle$  transition with Rabi frequency  $\Omega/2$ . With the inclusion of this term the Hamiltonian now reads:

$$\begin{aligned} \hat{H}_{\text{ions}} = & \frac{\omega_0}{2} \sum_{j=1}^N \hat{\sigma}_{z,j} + \omega \hat{a}^\dagger \hat{a} + \frac{\Omega}{2} \sum_{j=1}^N \hat{\sigma}_{x,j} \\ & + \frac{V}{2\sqrt{N}} \sum_{j=1}^N [\hat{\sigma}_{+,j} ((1+\epsilon)\hat{a} + \hat{a}^\dagger) + \hat{\sigma}_{-,j} ((1+\epsilon)\hat{a}^\dagger + \hat{a})] \end{aligned} \quad (5.2)$$

and the time evolution of the system can again be found by the master equation approach as in last chapter and the equations of motion is now given by:

$$\dot{A} = -\frac{iV}{2\sqrt{N}} ((2+\epsilon)J_x - i\epsilon J_y) - i\omega A \quad (5.3)$$

$$\dot{J}_x = -\frac{\omega_0}{2} J_y + \frac{iV\epsilon}{2\sqrt{N}} J_z (A - A^*) - \frac{\gamma}{2} J_x \quad (5.4)$$

$$\dot{J}_y = -\frac{\Omega}{2} J_z + \frac{\omega_0}{2} J_x - \frac{V}{2\sqrt{N}} J_z (2+\epsilon) (A + A^*) - \frac{\gamma}{2} J_y \quad (5.5)$$

$$\dot{J}_z = \frac{\Omega}{2} J_y + \frac{V}{2\sqrt{N}} J_y (2+\epsilon) (A + A^*) - \frac{iV\epsilon}{2\sqrt{N}} J_x (A - A^*) - \gamma \left( J_z + \frac{1}{2} \right). \quad (5.6)$$

This section will investigate the steady state solutions of above equations, as was the case in the last chapter.

## 5.2 Fluctuations

As in previous section this section adds the driving term to the derivation of the fluctuations from section (4.3) and the equations describing the linearized time evolution of the fluctuations will with this addition be given by:

$$\frac{d\delta\hat{A}}{dt} = -\frac{iV}{2\sqrt{N}} \left[ (2+\epsilon)\delta\hat{J}_x - i\epsilon\delta\hat{J}_y \right] - i\omega\delta\hat{A} \quad (5.7)$$

$$\frac{d\delta\hat{A}^*}{dt} = \frac{iV}{2\sqrt{N}} \left[ (2+\epsilon)\delta\hat{J}_x + i\epsilon\delta\hat{J}_y \right] + i\omega\delta\hat{A}^* \quad (5.8)$$

$$\frac{d\delta\hat{J}_x}{dt} = -\frac{\omega_0}{2}\delta\hat{J}_y + \frac{iV\epsilon}{2\sqrt{N}}\delta\hat{J}_z(A-A^*) + \frac{iV\epsilon}{2\sqrt{N}}J_z(\delta\hat{A}-\delta\hat{A}^*) - \frac{\gamma}{2}\delta\hat{J}_x \quad (5.9)$$

$$\begin{aligned} \frac{d\delta\hat{J}_y}{dt} = & -\frac{\Omega}{2}\delta\hat{J}_z + \frac{\omega_0}{2}\delta\hat{J}_x - \frac{V}{2\sqrt{N}}\delta\hat{J}_z(2+\epsilon)(A+A^*) \\ & - \frac{V}{2\sqrt{N}}J_z(2+\epsilon)(\delta\hat{A}+\delta\hat{A}^*) - \frac{\gamma}{2}\delta\hat{J}_y \end{aligned} \quad (5.10)$$

$$\begin{aligned} \frac{d\delta\hat{J}_z}{dt} = & \frac{\Omega}{2}\delta\hat{J}_y + \frac{V}{2\sqrt{N}}\delta\hat{J}_y(2+\epsilon)(A+A^*) + \frac{V}{2\sqrt{N}}J_y(2+\epsilon)(\delta\hat{A}+\delta\hat{A}^*) \\ & - \frac{iV\epsilon}{2\sqrt{N}}\delta\hat{J}_x(A-A^*) - \frac{iV\epsilon}{2\sqrt{N}}J_x(\delta\hat{A}-\delta\hat{A}^*) - \gamma\delta\hat{J}_z. \end{aligned} \quad (5.11)$$

### 5.3 $J_z$ -polynomial

In the previous chapter  $\Omega$  was neglected except in figure (4.3), where it was shown how a term  $\Omega\hat{\sigma}_x$  could split the degeneracy of one of the null points in the  $J_z$ -polynomial. This term was included already there to show one possible benefit of the inclusion of a driving term. Equation (4.15) for the  $J_z$ -polynomial without  $\Omega$  is changed into equation (5.12) with the inclusion of the driving term.

$$\begin{aligned} 0 = & -\left(J_z + \frac{1}{2}\right) [2\gamma\delta^2 J_z^4 + 4\beta\delta\gamma J_z^3 + 2\gamma\alpha^2] \\ & -\left(J_z + \frac{1}{2}\right) [4\gamma\alpha\beta J_z + 4\gamma\alpha\delta J_z^2 + 2\gamma\beta^2 J_z^2] \\ & + [\Omega^2\gamma\omega\beta + (2+\epsilon)^2 V^2 \Omega^2 \gamma\omega\omega_0/N - V^2 \epsilon^2 \gamma\omega\omega_0 \Omega^2/N] J_z^2 \\ & + [\Omega^2\gamma\omega\delta - V^4 \epsilon^4 \Omega^2 \gamma/N^2 + \Omega^2\gamma(2+\epsilon)^2 V^4 \epsilon^2/N^2] J_z^3 + \Omega^2\gamma\omega\alpha J_z, \end{aligned} \quad (5.12)$$

where

$$\alpha = \omega [\omega_0^2 + \gamma^2], \quad \beta = V^2 \omega_0 [\epsilon^2 + (2 + \epsilon)^2] / N, \quad \delta = (2 + \epsilon)^2 V^4 \epsilon^2 / \omega N^2 \quad (5.13)$$

In figure (5.1) a  $J_z$ -polynomial is shown where a driving term  $\Omega$  of same magnitude as the other parameters is included (in contrast to the  $J_z$ -polynomials in section (4.1.2)). It is seen how the  $J_z$ -values of  $V\sqrt{N} = 0.16$  has changed from  $-N/2$  to around  $-0.2N$  for the null point, but there is still only one solution for this value of  $V$ . For larger  $V$ 's three solutions are shown, the doubledegeneracy is hence lifted and the values of  $J_z$  is split. It is also seen that the splitting between the second and third null point at some point starts to shrink and for even larger values of  $V$  the knot will be below zero and there are only one null point again. The symbolic solve approach finds the solutions easier with the inclusion of  $\Omega$ , but it is more difficult for the fsolve approach. The numerics run hence faster for  $\epsilon = 0$  in which case matlab was able to solve the steady state equations symbolic.

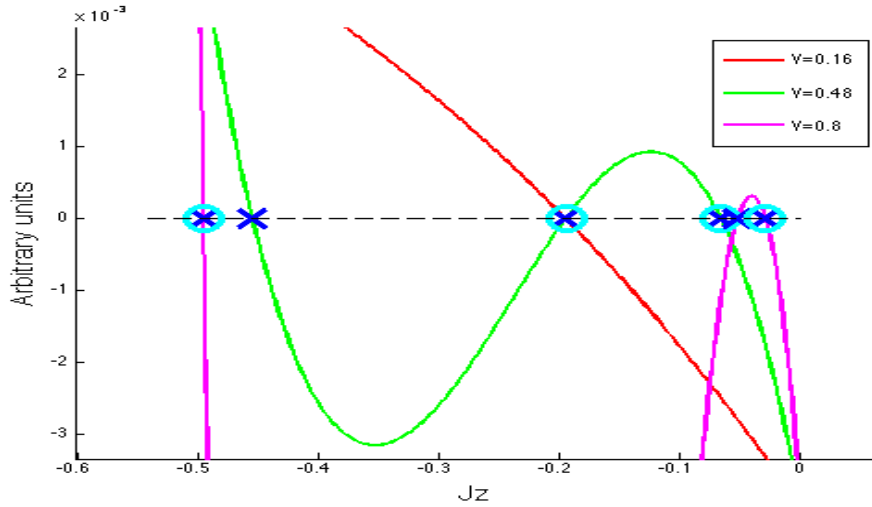


Figure 5.1: Parameters:  $\epsilon = 0.0, \omega = 0.5, \omega_0 = 0.1, \Omega = 0.20$ . Red: analytical solution without  $\epsilon$ . Blue with  $\epsilon$ . Both without  $\Omega$ .

## 5.4 Regime 1: $\omega_0 \neq 0$

This section presents how the phase diagram is changed from what was seen in chapter (4) when one includes a driving term  $\Omega \hat{\sigma}_x$  of comparable magnitude with the ions splitting energy. The figures are produced in the same manner as in previous chapter, just with new parameters.

### 5.4.1 Phase Diagrams

In figure (5.2) a phase diagram is shown with the same parameter values as used in chapter (4), but with the inclusion of a driving term  $\Omega = 0.2$ . It is seen that the phase boundary is moved out in the sense that a larger dissipation term is needed in order to compete with the  $\hat{x}$ -direction. The same chaotic phase which was seen in the previous chapter is still included. Save for this change of where the phase boundary is nothing new is immediately added to the phase diagram, even for relative large values of  $\Omega$  (see figure (5.4(a)+5.4(b))). The green dashed line indicate where the phase boundary were with the same parameter values, but with  $\Omega = 0$ , according to equation (4.21).

In figure (5.3) the same plot as the one shown in figure (5.2) but where the points have been found with matlab's `fsolve` instead of the `ode45`. The same overall behaviour is seen in both figures, but in the `fsolve` figure an odd line is shown. This will be discussed further in section (5.4.2).

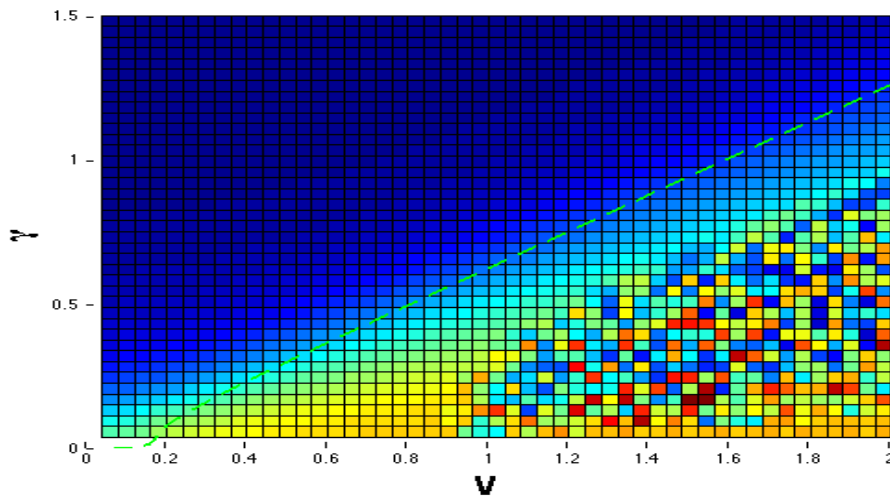


Figure 5.2: Parameters:  $\epsilon = 0.0, \omega = 0.5, \omega_0 = 0.1, \Omega = 0.20$ . Red: analytical solution without  $\epsilon$ . Blue with  $\epsilon$ . Both without  $\Omega$ .

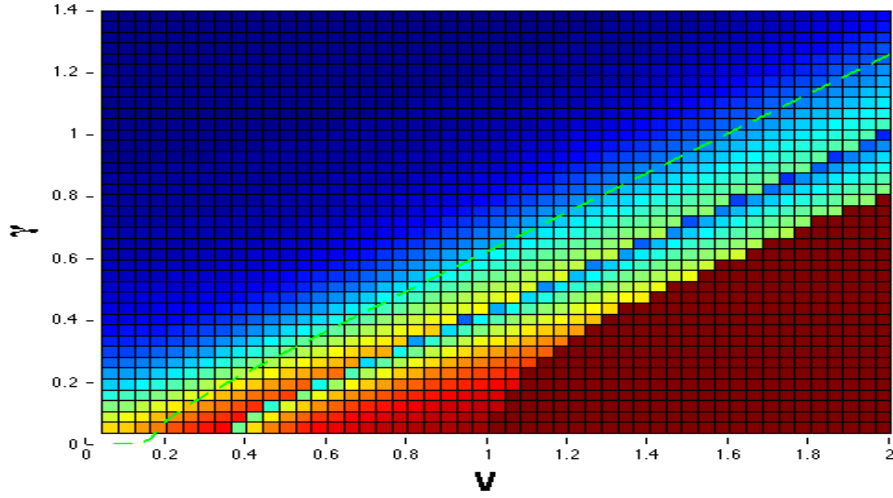


Figure 5.3: Parameters:  $\epsilon = 0.0, \omega = 0.5, \omega_0 = 0.1, \Omega = 0.20$ . solve approach

Two other examples are shown here:

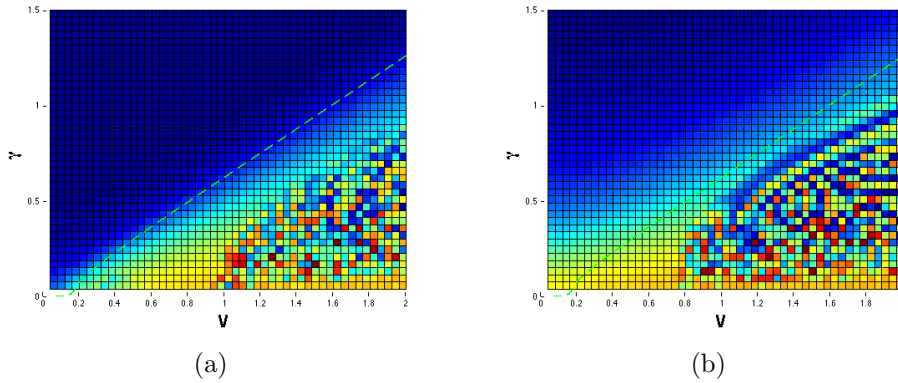


Figure 5.4: Parameters:  $\epsilon = 0.0, \omega = 0.5, \omega_0 = 0.1$  and left  $\Omega = 0.10$  and right  $\Omega = 0.50$

### 5.4.2 Number of (stable) solutions

This section presents three set of two figures, each set consists of a figure with the number of solutions and a figure with the number of stable solutions. In contrast to previous section it is clear that the inclusion of  $\Omega$  not only changes the position of the phase boundary but alters the underlying physics. At the boundary between the superradiant and chaotic phase there is *one* stable solution in contrast to the superradiant (with two stable solution) and the

chaotic phase (with zero stable solutions) and for  $\Omega = 0.5$  a new area with no stable solutions arise.

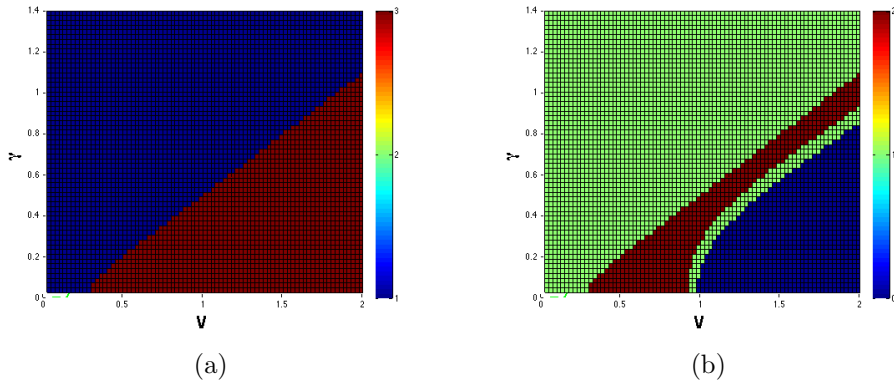


Figure 5.5: Parameters:  $\epsilon = 0.0, \omega = 0.5, \omega_0 = 0.1, \Omega = 0.10$ . Left number of solutions, right number of stable solutions.

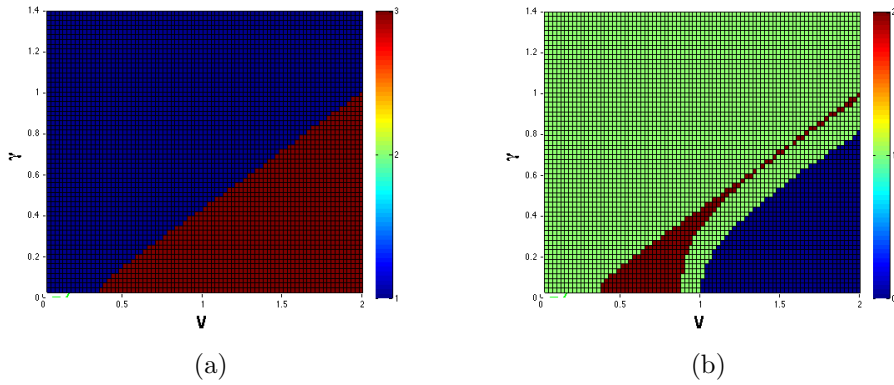


Figure 5.6: Parameters:  $\epsilon = 0.0, \omega = 0.5, \omega_0 = 0.1, \Omega = 0.20$ . Left number of solutions, right number of stable solutions.

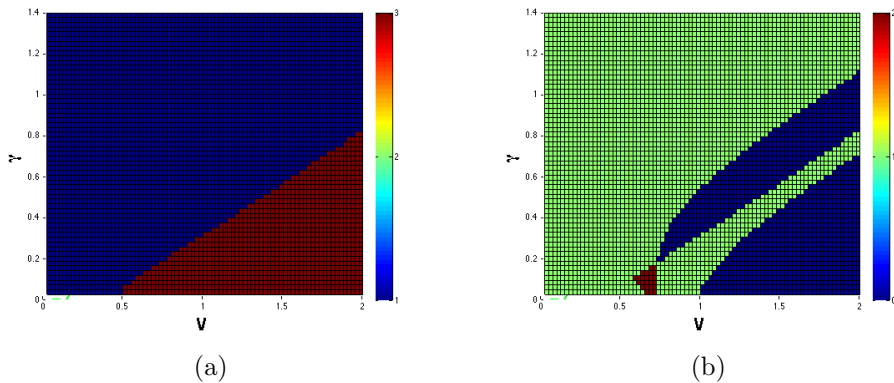


Figure 5.7: Parameters:  $\epsilon = 0.0, \omega = 0.5, \omega_0 = 0.1, \Omega = 0.50$ . Left number of solutions, right number of stable solutions.

### 5.4.3 $J_z(t)$ -graphs

In this section four points from figure (5.6(b)) is shown, they are indicated with red dots (MISSES) and are chosen because they represent the four different regimes seen for  $\gamma = 0.1$ .

It is seen in figures (5.8(a)-5.8(d)) that the areas which in the standard Dicke model was referred to as normal and superradiant phase dampens and the system develop into a steady state. In the newly arisen area between the superradiant and chaotic phase the system keeps oscillating even for large time intervals. This might be due to the fact that it is around a phase transition where the relaxation time is much longer and the system only for very large time scales dampens. This explain why the previous section showed there exist one stable solutions and why a new line was shown in the middle of the superradiant phase in figure (5.3). The time evolution in the chaotic regime is still chaotic as seen in previous chapter.

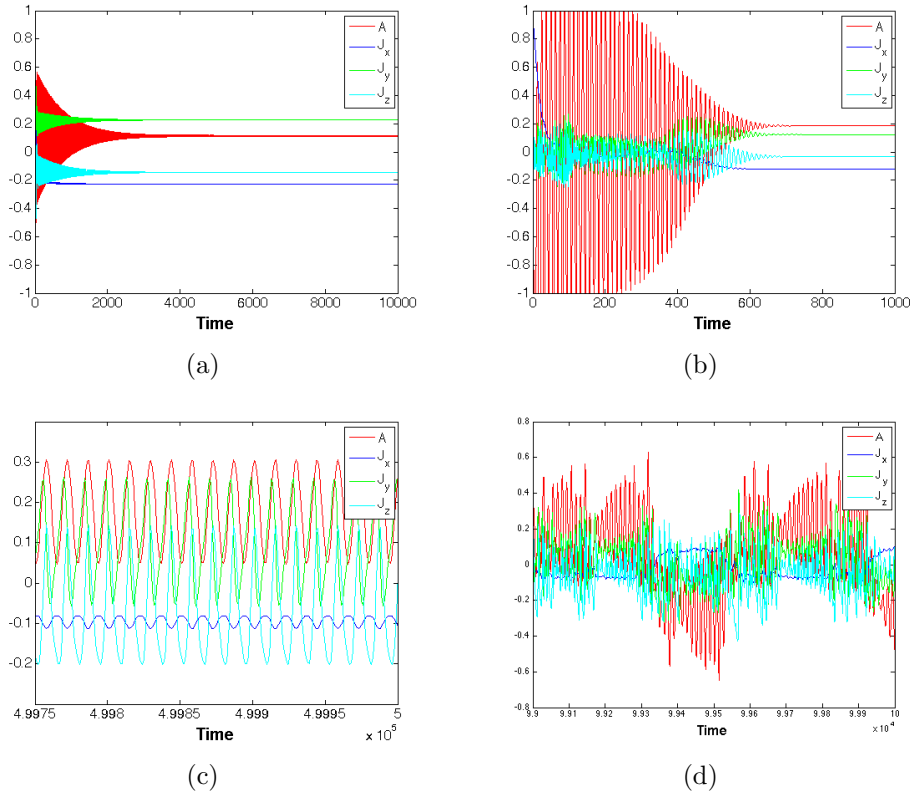


Figure 5.8: Parameters:  $\epsilon = 0.0, \omega = 0.5, \omega_0 = 0.1, \Omega = 0.0, \gamma = 0.1$ . Left up:  $V = 0.25$  Left down:  $V = 0.95$  Right up:  $V = 0.75$  Right down:  $V = 1.5$ .

#### 5.4.4 Stability

The path along the two lines shown in figure (5.6(b)) (MISSES) are here taken and the largest real value from the eigenvalues from the matrix describing the time evolution of the fluctuations is shown in figures (5.9+5.10). From here it is seen that the normal and superradiant phase are stable and the chaotic and new region between superradiant and chaotic phase have unstable and stable regions.

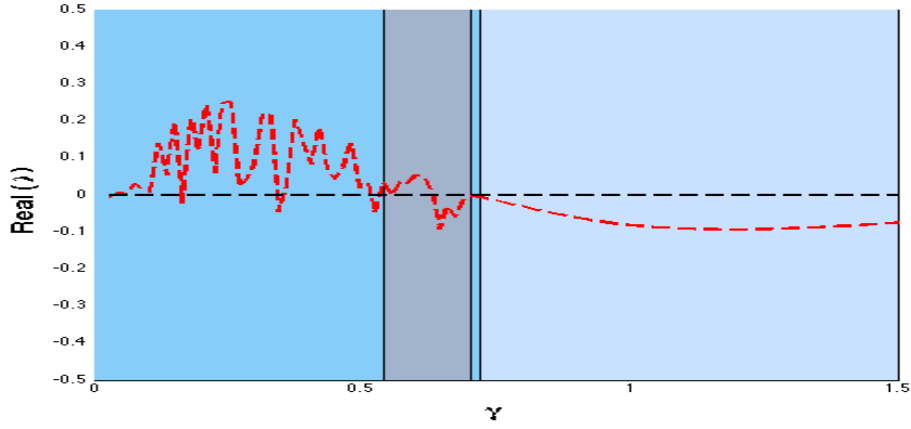


Figure 5.9: Parameters:  $\epsilon = 0.0, \omega = 0.5, \omega_0 = 0.1, \Omega = 0.2, V = 1.5$ .

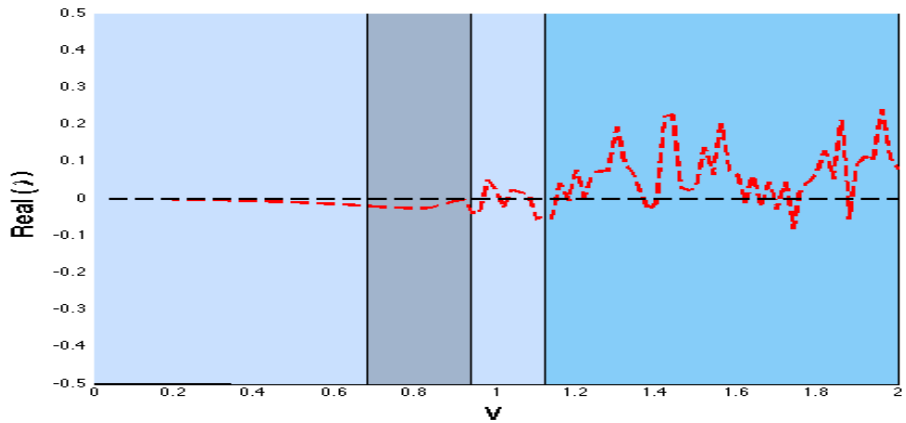


Figure 5.10: Parameters:  $\epsilon = 0.0, \omega = 0.5, \omega_0 = 0.1, \Omega = 0.2, \gamma = 0.25$ .

## 5.5 Regime 2: $\omega_0 = 0, \epsilon \neq 0$

In the first part of this chapter it was shown how the introduction of a driving term  $\Omega\hat{\sigma}_x$  of same magnitude as the parameters used in chapter (4) adds a new region between the superradiant and chaotic phase compared to the standard Dicke model.

In this second part of this chapter a new regime is investigated; the regime where one can neglect the ionic term  $\omega_0$ . This regime is investigated in two parts, one with inclusion of the sideband cooling parameter  $\epsilon$  (this section) and one without (section (5.6)).

### 5.5.1 Phase Diagrams

In figure (5.11) a phase diagram is shown in the regime where the ionic term is neglected and sideband cooling is included. A first order phase transition is seen when one scan over  $\gamma$  for values of  $V$  above about 0.4. For  $V < 0.4$  it is not obvious from the phase diagram what happens.

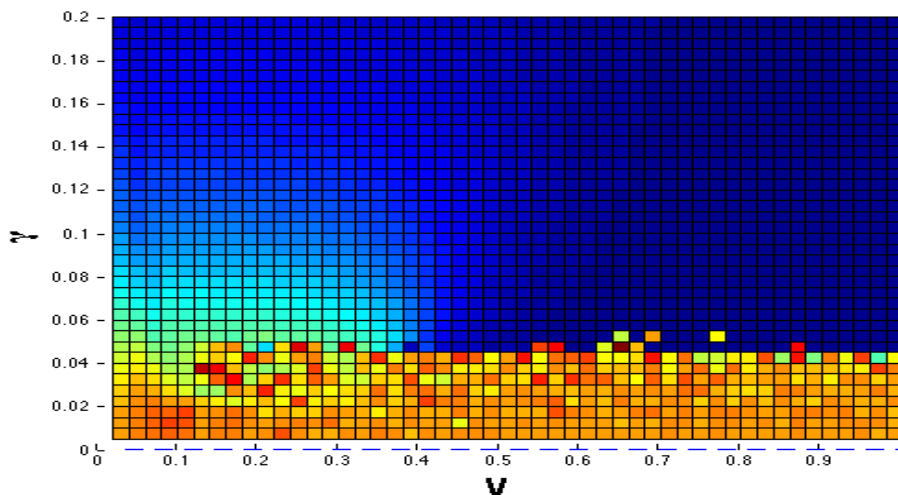


Figure 5.11: Parameters:  $\epsilon = 0.05, \omega = 0.1, \omega_0 = 0.0, \Omega = 0.1$ . Red: analytical solution without  $\epsilon$ . Blue with  $\epsilon$ . Both without  $\Omega$ .

In order to get an understanding of what goes on figures (5.12(a)-5.12(d)) show the time evolution of the collective angular momentum operators for different points in the phase diagram (indicated with small green crosses in the phase diagram). This is followed by figures () which shows the largest real part of the eigenvalues of the matrix describing the fluctuations (analogously to XX in section YY).

NEW

This phase diagram will be investigated by the tools described in the previous chapter. Four points indicated with green crosses will be chosen for further analysis and they will be described in the following subsections, each named after whether the values of  $\gamma$  and  $V$  are relatively small or large.

### 5.5.2 $J_z(t)$ -graphs

Figures in this section are split into subsections depending on the regime

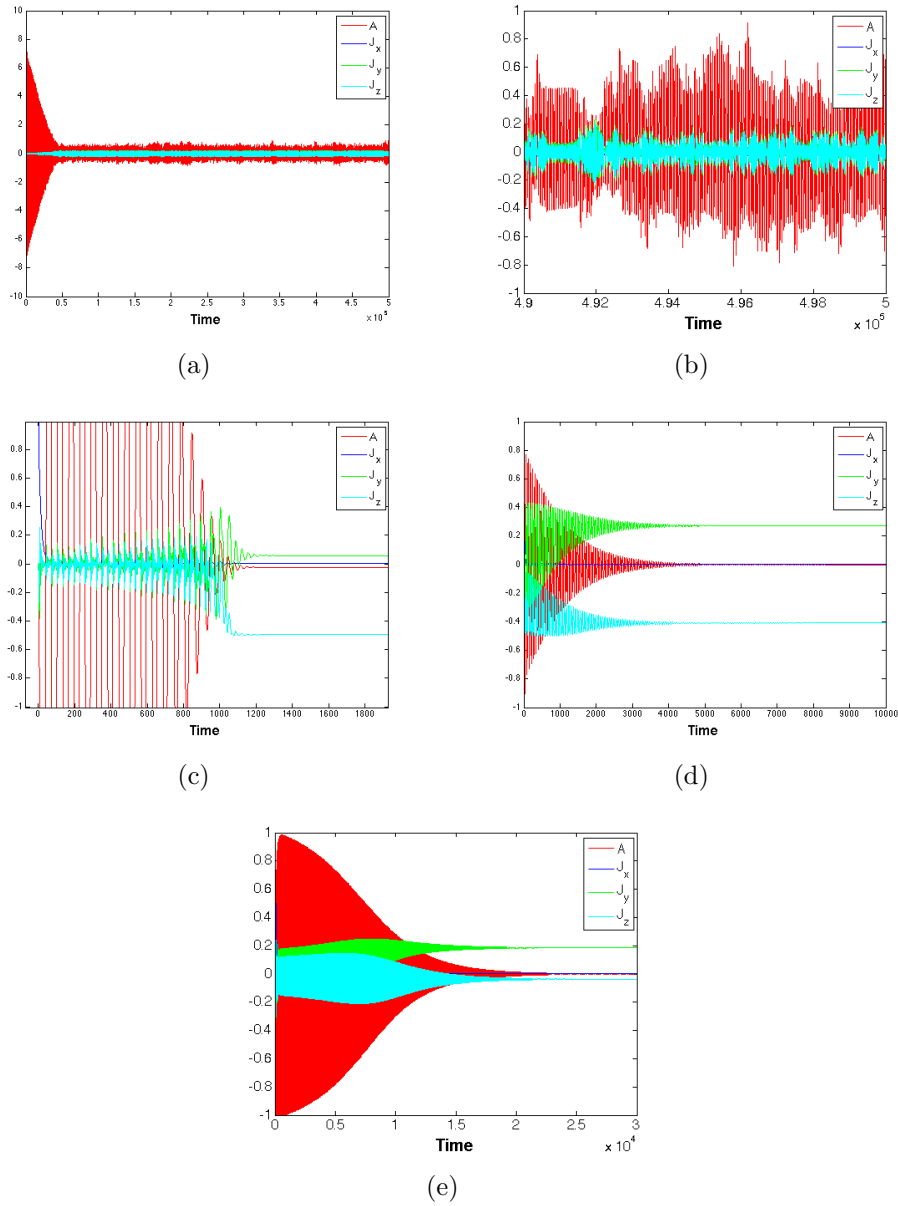


Figure 5.12: Parameters:  $\epsilon = 0.05, \omega = 0.1, \omega_0 = 0.0, \Omega = 0.1$ . 5.12(a):  $\gamma = 0.02, V = 0.8$ , 5.12(b):  $\gamma = 0.02, V = 0.8$  (zoom of 5.12(a)), 5.12(c):  $\gamma = 0.15, V = 0.8$ , 5.12(d):  $\gamma = 0.15, V = 0.1$ , 5.12(e):  $\gamma = 0.02, V = 0.1$

### 5.5.3 Real values of eigenvalues of fluctuations

In this subsection four different paths are taken in the phase diagram shown in figure (5.11), connecting the four points indicated with green crosses. In

each scan the largest real part of the eigenvalues of the matrix describing the time evolution of the fluctuations is shown.

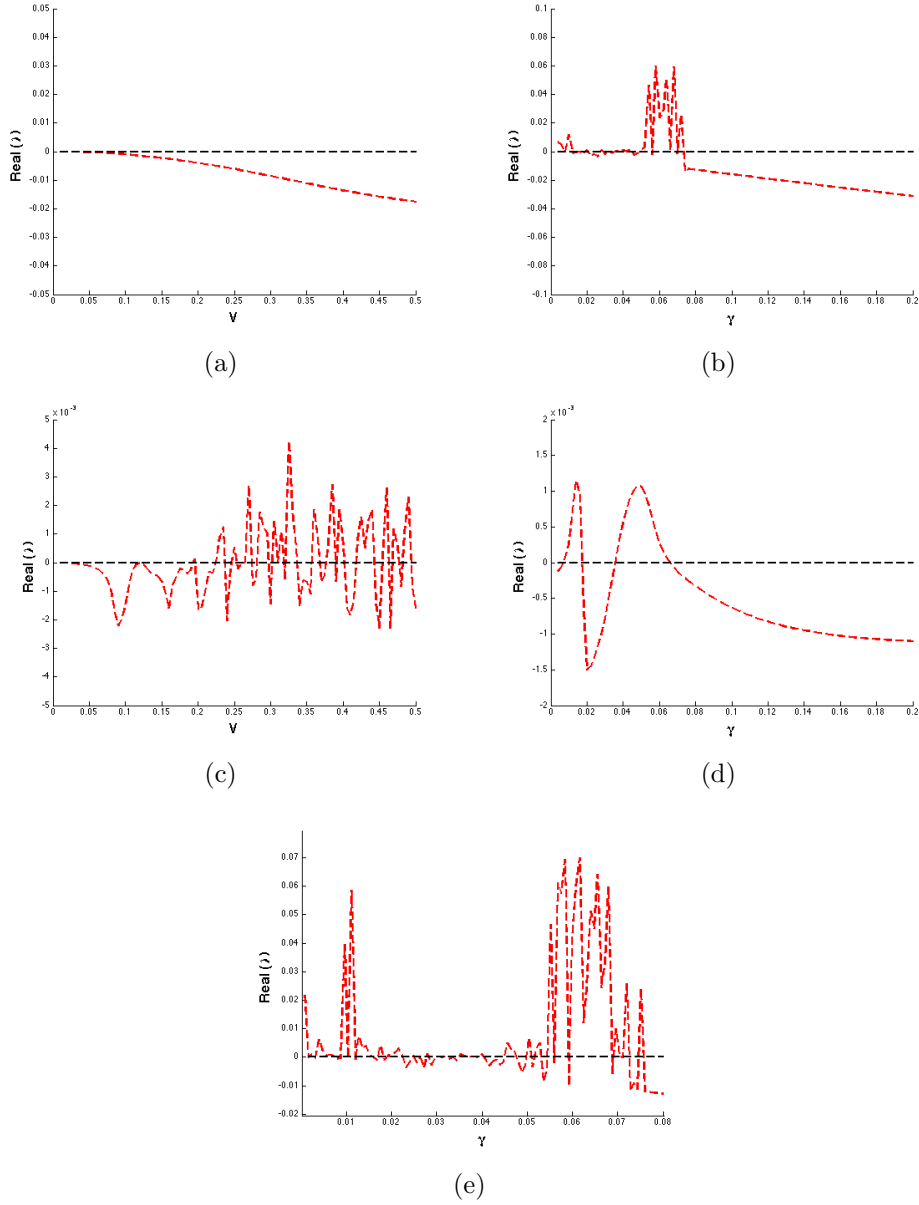


Figure 5.13: Parameters:  $\epsilon = 0.05, \omega = 0.1, \omega_0 = 0.0, \Omega = 0.1$ . 5.13(a):  $\gamma = 0.15$ , 5.13(b):  $V = 0.8$ , 5.13(c):  $\gamma = 0.02$ , 5.13(d):  $V = 0.1$ , 5.13(e): zoom of 5.13(b).

Scan over  $\gamma$ ,  $V$  small  $V, \gamma$

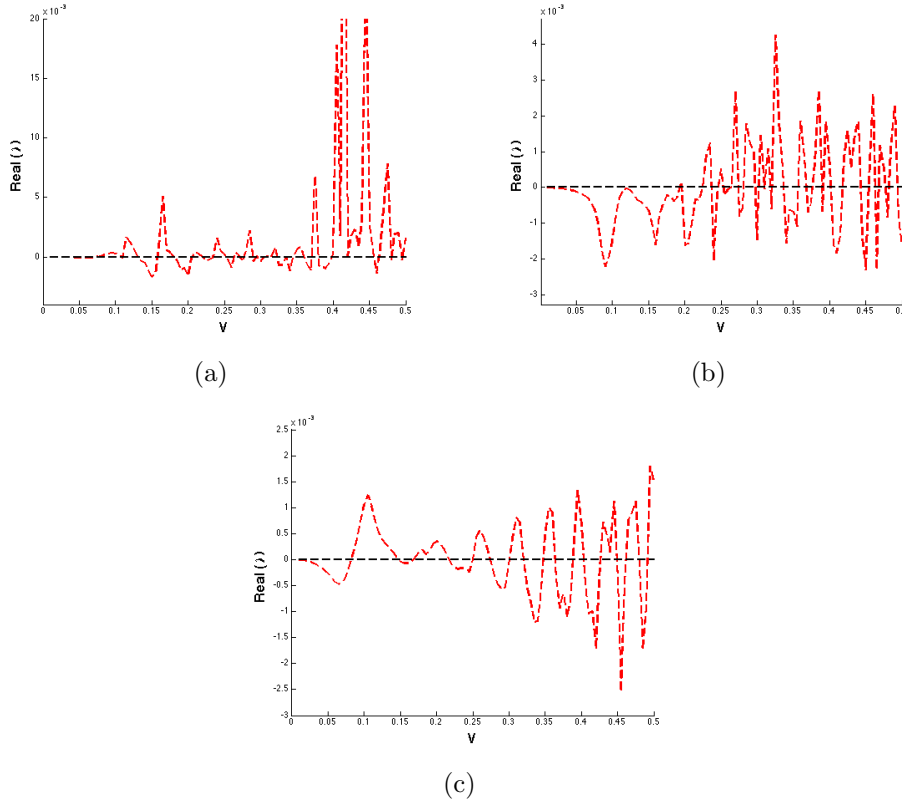


Figure 5.14: Parameters:  $\epsilon = 0.05, \omega = 0.1, \omega_0 = 0.0, \Omega = 0.1$ . 5.14(a):  $\gamma = 0.01$ , 5.14(b):  $\gamma = 0.02$ , 5.14(c):  $\gamma = 0.05$

## 5.6 Regime 3: $\omega_o = 0, \epsilon = 0$

In previous subsection the regime with neglectable  $\omega_0$ -term was investigated with the inclusion of sideband cooling in form of the  $\epsilon$  parameter. In figure (5.15) a phase diagram is shown in the same regime, but with  $\epsilon = 0$ .

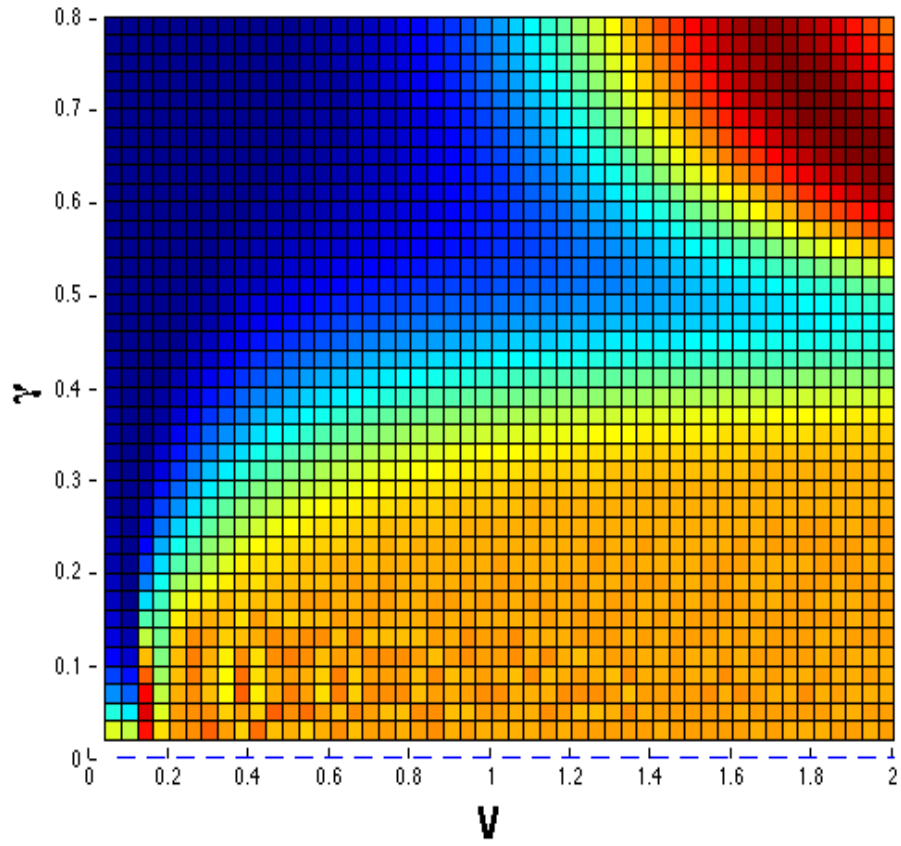


Figure 5.15: Parameters:  $\epsilon = 0.0, \omega = 0.1, \omega_0 = 0.0, \Omega = 0.1$ .

# Chapter 6

## The chaotic regime

Write something in general about chaos and this phase

### 6.1 Chaotic behaviour in small time scales

In section (4.3.2) and for instance figure (4.24) in the chaotic phase it is seen that the largest real part of the eigenvalues of the matrix representing the time evolution of the fluctuations sometimes are positive and sometimes negative. It is hence clear that for some values of  $V$  and  $\gamma$  there are stable solutions in the chaotic phase. (does this have a name?)

This behaviour is not covered in either the ode45 or the fsolve approach, see figures (4.5+4.6). In figure () a zoom of the chaotic phase is shown. In this zoom the steps in  $V$  in the phase diagram are much smaller ( $\Delta V = 0.001$  compared to  $\Delta V = 0.025$ ). It is here seen that for small steps the stable solutions in the chaotic phase are included.

### 6.2 Strange attractors

In figures (6.1+6.2) a plot of the phase diagram with the inclusion of a driving term  $\Omega = 1.0$  where each point origin from the ode45 approach. The difference between the two plots is the number of iterations made. It is clear that they give similar results. In extension to the chaotic behaviour which have been seen previously they also show regions with strange attractors, see next section.

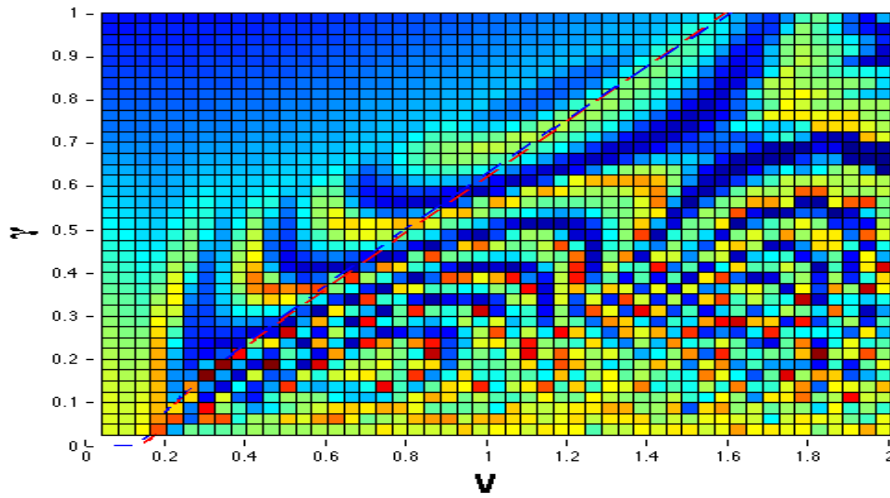


Figure 6.1: Parameters:  $\epsilon = 0.05, \omega = 0.5, \omega_0 = 0.1, \Omega = 1.0$ . Red: analytical solution without  $\epsilon$ . Blue with  $\epsilon$ . Both without  $\Omega$ . Number of iterations (ode45) changed to 3,000. Initial condition  $J_x = 1$

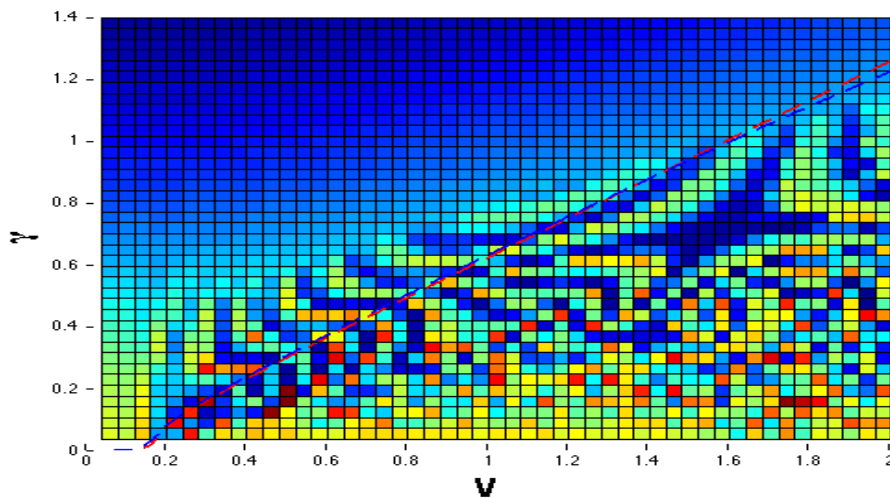


Figure 6.2: Parameters:  $\epsilon = 0.05, \omega = 0.5, \omega_0 = 0.1, \Omega = 1.0$ . Red: analytical solution without  $\epsilon$ . Blue with  $\epsilon$ . Both without  $\Omega$ . Number of iterations (ode45) changed to 5,000. Initial condition  $J_x = 1$

explain strange attractors/Lyapunov?  
 show zoom of the graphs  
 chaos regime increases with Omega possible to get these transition occurrence with Omega (to be in section chaos?) include a graph with small

*Omega*

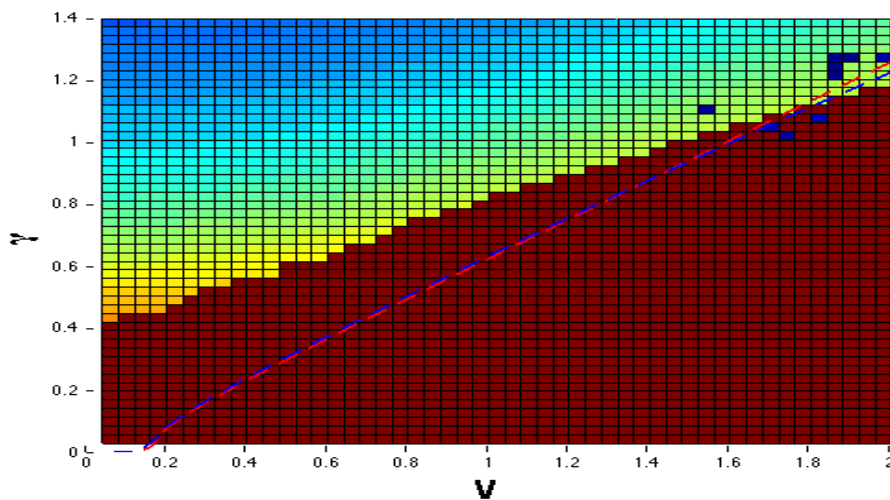


Figure 6.3: Parameters:  $\epsilon = 0.0, \omega = 0.5, \omega_0 = 0.1, \Omega = 1.000$ . Red: analytical solution without  $\epsilon$ . Blue with  $\epsilon$ . Both without  $\Omega$ .

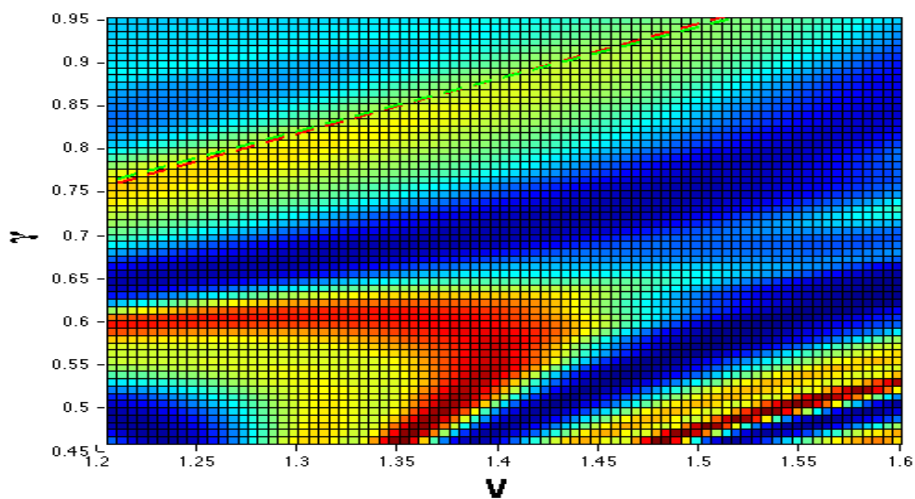


Figure 6.4: Parameters:  $\epsilon = 0.05, \omega = 0.5, \omega_0 = 0.1, \Omega = 1.000$ . Red: analytical solution without  $\epsilon$ . Blue with  $\epsilon$ . Both without  $\Omega$ .

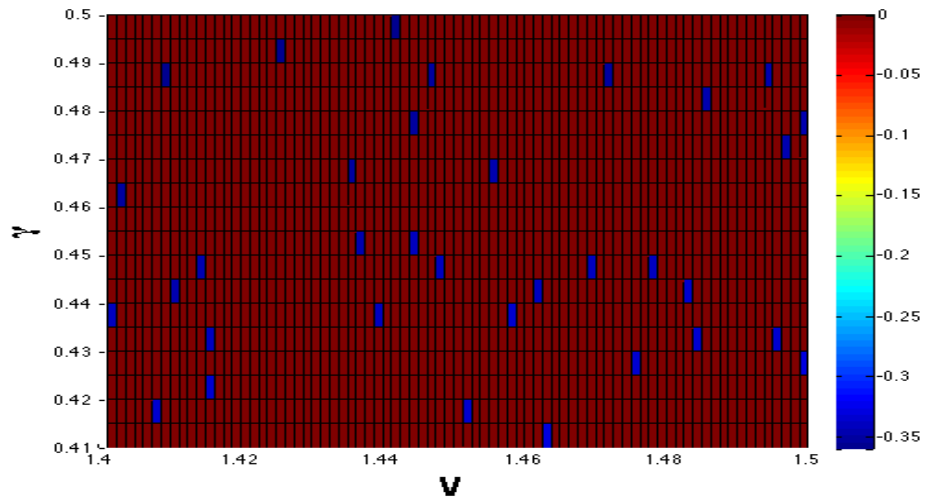


Figure 6.5: Parameters:  $\epsilon = 0.0, \omega = 0.5, \omega_0 = 0.1, \Omega = 1.000$ . Red: analytical solution without  $\epsilon$ . Blue with  $\epsilon$ . Both without  $\Omega$ . fsolve

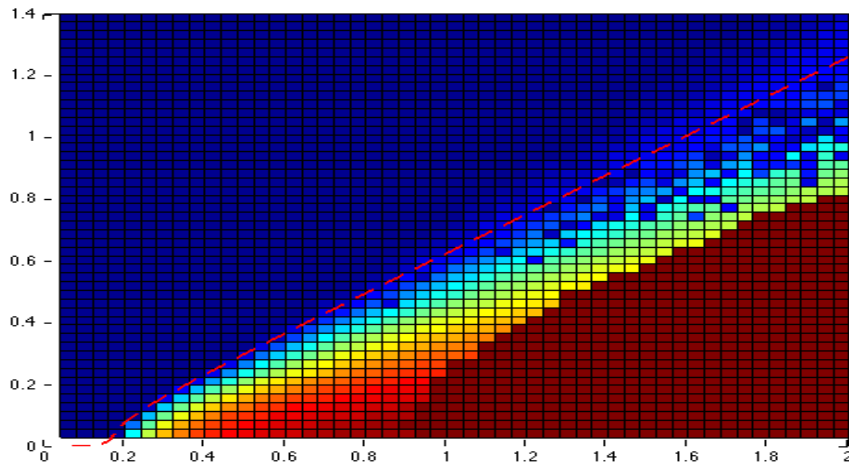


Figure 6.6: Parameters:  $\epsilon = 0.05, \omega = 0.5, \omega_0 = 0.1, \Omega = 0.0$ .

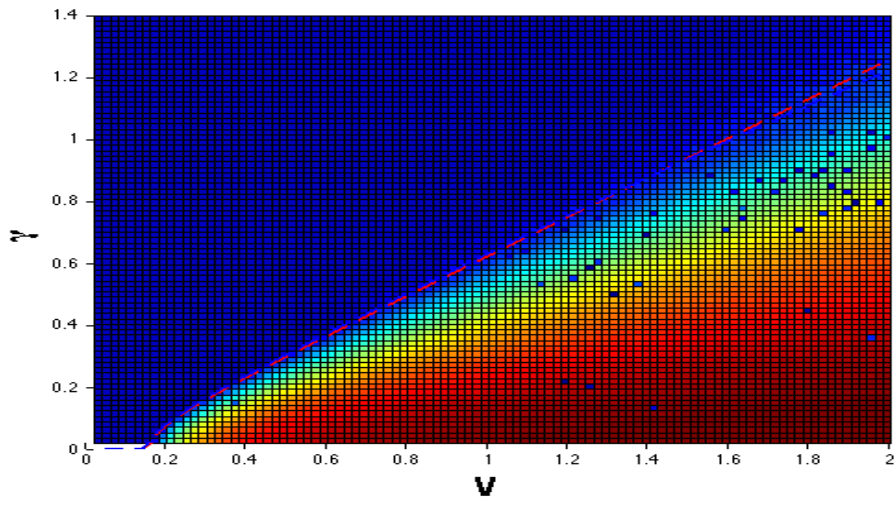


Figure 6.7: Parameters:  $\epsilon = 0.05, \omega = 0.5, \omega_0 = 0.1, \Omega = 0.0$ . *fsolve*

# Chapter 7

## Conclusion and Outlook

### 7.1 Conclusion

This thesis has overall three different schemes it has investigated; the standard Dicke model, an observed chaotic phase when one includes dissipation to the standard Dicke model and an extended Dicke model where a driving term has been included.

#### 7.1.1 The Standard Dicke Model

The standard Dicke model was investigated with inclusion of dissipation. It has been shown the phase diagrams are time independent and the the approach to seek steady state solutions is hence a satisfactory approach, except for an observed chaotic phase.

First of all has the second order phase transition known for the standard Dicke model been observed, where the phase boundary for the simulation follows the analytical expression and a critical value for  $V$  is found, where no phase transition occurs for values of  $V < V_{\text{critical}}$ . This was as expected and has been observed previously.

The system has been shown to have stable solutions in the normal and super-radiant phase. One solution which is stable in the normal and three solution of which two are stable in the super-radiant phase.

This phase transition also induce a broken symmetry, where  $J_x, J_y$  and  $A$  goes from the normal phase with only one solution to a superradiant phase, where they can have different values. In the superradiant phase three solutions exist, but only two of them are stable. Which state the system ends in

depends on the initial conditions.

The Hamiltonian used in this thesis two extra terms to the standard Dicke model was introduced. One of the term  $\epsilon$  models the sideband cooling and  $\Omega$  is an extra driving term. In the case where sideband cooling has been added to the standard Dicke model this thesis has shown that this increase the stability of the system, but it also alters the phase diagrams. When  $\epsilon$  is included not only a lower bound (the mentioned  $V_{\text{critical}}$ ) exists, but also an upper bound occur. For values of  $V > V_{\text{upper bound}}$  no phase transition occurs (as in the case of  $V < V_{\text{lower bound}}$ ).

### 7.1.2 The Extended Dicke Model

In the case where a driving term  $\Omega$  is added to the standard Dicke model two different regimes has been investigated. First in the case where the driving term is on the same magnitude as the terms used in the analysis of the standard Dicke model. Here it was shown that the inclusion of a driving term only changes the position of the phase boundary - it smoothens the phase transitions further out, but leave the system otherwise unchanged, save for a further break of symmetry. In the standard Dicke model the phase transition from a normal to a superradiant phase induced a broken symmetry, but the values of for instance  $J_x$  in the stable solutions in the superradiant phase were  $\pm x$ , where  $x$  is the value of  $J_x$  for a given set of parameters. The inclusion of  $\Omega$  removes this symmetry. This was also seen in the  $J_z$ -polynomials where the inclusion of  $\Omega$  lifts the degeneracy of one of the solutions.

Secondly a regime with a neglectable ionic  $\omega_0 = 0$ . Here the phase diagram strongly depends on whether sideband cooling is included or not. In the case with inclusion of sideband cooling a first order phase transition is observed between a stable normal phase and a unstable superradiant phase. But the existence of the phase transition depends on the parameters and for values below a critical  $V_{\text{critical}}$  no phase transition occur. It is possible to go from one state to the other by going around this critical point.

In the case without sideband cooling, but still in the regime  $\omega_0 = 0$  an interesting, but unfortunately not well understood phase diagram comes out.

### 7.1.3 The Chaotic Phase

In addition to the normal and superradiant phase known for the standard Dicke model a chaotic phase was also observed. In the chaotic phase no sta-

ble solutions exist and the values of for instance  $J_z$  keeps fluctuating. The values saved if one simulates the evolution of the system is hence random as seen in the  $J_z(t)$  figures.

The chaotic phase for the extended Dicke model with relatively large values of  $\Omega$  exhibit an interesting new phenomena, which could be a strange attractor.

## 7.2 Outlook

This thesis has shown the existence of different phases and first and second order phase transitions, critical points, etc.

If one should investigate this further it would be obvious to check whether the states are squeezed, as in the case of Johathan Home. It would also be obvious to try to see how the system develops for a finite number of ions. Jonathan Home is currently able to make this experiment with *one* ion, but could make it with 2-3 ions. The experimental group in Innsbruck has also a setup which is covered by the Hamiltonian described by this thesis and can realize this experiment with 5 ions.

It would also be of huge interest to understand the phases seen in the chapter about the extended Dicke model. This thesis has been able to show XX, but further questions arise, such as XX.

This thesis has investigated the standard Dicke model and how the physics of the system change for an extension..

This thesis has shown the known second order phase transition in the Dicke model.

- 2<sup>nd</sup> order phase transition and analytical expression for the phase boundary  $\gamma(V)$  and the critical  $V$
- Shown upper limit on  $V$  if  $\epsilon$  is included
- Shown a chaotic phase
- Jz-T graph chaotic phase
- Broken symmetry
- Fluctuations, linearization and epsilon, stable solutions
- chaotic phase: small and large Omega + strange attractors
- extended ...'0

# Appendix A

## Mean field equations

The Hamiltonian of the system is given by

$$\hat{H}_{\text{ions}} = \frac{\omega_0}{2} \sum_{j=1}^N \hat{\sigma}_{z,j} + \omega \hat{a}^\dagger \hat{a} + \frac{\Omega}{2} \sum_{j=1}^N \hat{\sigma}_{x,j} \quad (\text{A.1})$$

$$+ \frac{V}{2\sqrt{N}} \sum_{j=1}^N [\hat{\sigma}_{+,j} ((1 + \epsilon) \hat{a} + \hat{a}^\dagger) + \hat{\sigma}_{-,j} ((1 + \epsilon) \hat{a}^\dagger + \hat{a})]. \quad (\text{A.2})$$

The time evolution of the system can be described by the master equation approach where an observable operator evolves according to [22]:

$$\frac{d\hat{x}}{dt} = i [\hat{H}_S, \hat{x}] + \mathcal{L}(\hat{x}), \quad (\text{A.3})$$

where  $\hbar = 1$ ,  $\hat{x}$  is the observable under study and the Liouvillian operator  $\mathcal{L}(\hat{x})$  can be expressed in the Heisenberg picture in which case it takes the form

$$\mathcal{L}(\hat{x}) = - \sum_k \frac{\gamma_k}{2} \left( \hat{c}_k^\dagger \hat{c}_k \hat{x} + \hat{x} \hat{c}_k^\dagger \hat{c}_k - 2 \hat{c}_k \hat{x} \hat{c}_k^\dagger \right) \quad (\text{A.4})$$

If one uses the ensemble variables  $J_i, A$  introduced in section (3.1.6) and investigates how they develop in time one can use the above approach. With  $\hat{c}_k = \hat{\sigma}_-$  and  $\gamma_k = \gamma$  one obtains the following for the operator  $J_x$  and in the following  $J_y, J_z$  and  $A$  as well.

$$J_x = \left\langle \sum_{j=1}^N \hat{\sigma}_{x,j} \right\rangle = i \left\langle \left[ H, \sum_{j=1}^N \hat{\sigma}_{x,j} \right] \right\rangle \quad (\text{A.5})$$

$$+ \left\langle \sum_{j=1}^N \frac{\gamma}{2} [2\hat{\sigma}_{+,j}\hat{\sigma}_{x,j}\hat{\sigma}_{-,j} - \hat{\sigma}_{+,j}\hat{\sigma}_{-,j}\hat{\sigma}_{x,j} - \hat{\sigma}_{x,j}\hat{\sigma}_{+,j}\hat{\sigma}_{-,j}] \right\rangle \quad (\text{A.6})$$

$$= i \left\langle \left[ \sum_{j=1}^N \left[ \frac{\omega_0}{2} \hat{\sigma}_{z,j} + \frac{iV\epsilon}{2\sqrt{N}} \hat{\sigma}_{y,j} (\hat{a} - \hat{a}^\dagger) \right], \sum_{j=1}^N \hat{\sigma}_{x,j} \right] \right\rangle \quad (\text{A.7})$$

$$+ \frac{\gamma}{2} \left\langle \sum_{j=1}^N [2\hat{\sigma}_{+,j}\hat{\sigma}_{x,j}\hat{\sigma}_{-,j} - \hat{\sigma}_{+,j}\hat{\sigma}_{-,j}\hat{\sigma}_{x,j} - \hat{\sigma}_{x,j}\hat{\sigma}_{+,j}\hat{\sigma}_{-,j}] \right\rangle \quad (\text{A.8})$$

$$= \left\langle \sum_{j=1}^N \left[ -\frac{\omega_0}{2} \hat{\sigma}_{y,j} + \frac{iV\epsilon}{2\sqrt{N}} \hat{\sigma}_{z,j} (\hat{a} - \hat{a}^\dagger) \right] \right\rangle \quad (\text{A.9})$$

$$- \frac{\gamma}{2} \left\langle \sum_{j=1}^N \hat{\sigma}_{x,j} \right\rangle \quad (\text{A.10})$$

$$= -\frac{\omega_0}{2} J_y + \frac{iV\epsilon}{2\sqrt{N}} J_z (A - A^*) - \frac{\gamma}{2} J_x \quad (\text{A.11})$$

$$\dot{J}_y = \left\langle \sum_{j=1}^N \dot{\sigma}_{y,j} \right\rangle = i \left\langle \left[ H, \sum_{j=1}^N \hat{\sigma}_{y,j} \right] \right\rangle \quad (\text{A.12})$$

$$+ \left\langle \sum_{j=1}^N \frac{\gamma}{2} [2\hat{\sigma}_{+,j}\hat{\sigma}_{y,j}\hat{\sigma}_{-,j} - \hat{\sigma}_{+,j}\hat{\sigma}_{-,j}\hat{\sigma}_{y,j} - \hat{\sigma}_{y,j}\hat{\sigma}_{+,j}\hat{\sigma}_{-,j}] \right\rangle \quad (\text{A.13})$$

$$= i \left\langle \left[ \sum_{j=1}^N \left[ \frac{\Omega}{2} \hat{\sigma}_{x,j} + \frac{\omega_0}{2} \hat{\sigma}_{z,j} \right], \sum_{j=1}^N \hat{\sigma}_{y,j} \right] \right\rangle \quad (\text{A.14})$$

$$+ i \left\langle \left[ \sum_{j=1}^N \left[ \frac{V}{2\sqrt{N}} \hat{\sigma}_{x,j} (2 + \epsilon) (\hat{a} + \hat{a}^\dagger) \right], \sum_{j=1}^N \hat{\sigma}_{y,j} \right] \right\rangle \quad (\text{A.15})$$

$$- \frac{\gamma}{2} \left\langle \sum_{j=1}^N \hat{\sigma}_{y,j} \right\rangle \quad (\text{A.16})$$

$$= \left\langle \sum_{j=1}^N \left[ -\frac{\Omega}{2} \hat{\sigma}_{z,j} + \frac{\omega_0}{2} \hat{\sigma}_{x,j} - \frac{V}{2\sqrt{N}} \hat{\sigma}_{z,j} (2 + \epsilon) (\hat{a} + \hat{a}^\dagger) \right] \right\rangle \quad (\text{A.17})$$

$$- \frac{\gamma}{2} \left\langle \sum_{j=1}^N \hat{\sigma}_{y,j} \right\rangle \quad (\text{A.18})$$

$$= -\frac{\Omega}{2} J_z + \frac{\omega_0}{2} J_x - \frac{V}{2\sqrt{N}} J_z (2 + \epsilon) (A + A^*) - \frac{\gamma}{2} J_y \quad (\text{A.19})$$

$$J_z = \left\langle \sum_{j=1}^N \hat{\sigma}_{z,j} \right\rangle = i \left\langle \left[ H, \sum_{j=1}^N \hat{\sigma}_{z,j} \right] \right\rangle \quad (\text{A.20})$$

$$+ \left\langle \sum_{j=1}^N \frac{\gamma}{2} [2\hat{\sigma}_{+,j}\hat{\sigma}_{z,j}\hat{\sigma}_{-,j} - \hat{\sigma}_{+,j}\hat{\sigma}_{-,j}\hat{\sigma}_{z,j} - \hat{\sigma}_{z,j}\hat{\sigma}_{+,j}\hat{\sigma}_{-,j}] \right\rangle \quad (\text{A.21})$$

$$= i \left\langle \left[ \sum_{j=1}^N \left[ \frac{\Omega}{2} \hat{\sigma}_{x,j} + \frac{V}{2\sqrt{N}} [\hat{\sigma}_{x,j}(2+\epsilon)(\hat{a} + \hat{a}^\dagger) + i\epsilon \hat{\sigma}_{y,j}(\hat{a} - \hat{a}^\dagger)] \right], \sum_{j=1}^N \hat{\sigma}_{z,j} \right] \right\rangle \quad (\text{A.22})$$

$$- \frac{\gamma}{2} \left\langle \sum_{j=1}^N (2\hat{\sigma}_{z,j} + \mathbb{1}) \right\rangle \quad (\text{A.23})$$

$$= \left\langle \sum_{j=1}^N \left[ \frac{\Omega}{2} \hat{\sigma}_{y,j} + \frac{V}{2\sqrt{N}} [\hat{\sigma}_{y,j}(2+\epsilon)(\hat{a} + \hat{a}^\dagger) - i\epsilon \hat{\sigma}_{x,j}(\hat{a} - \hat{a}^\dagger)] \right] \right\rangle \quad (\text{A.24})$$

$$- \frac{\gamma}{2} \left\langle \sum_{j=1}^N (2\hat{\sigma}_{z,j} + \mathbb{1}) \right\rangle \quad (\text{A.25})$$

$$= \frac{\Omega}{2} J_y + \frac{V}{2\sqrt{N}} J_y (2+\epsilon) (A + A^*) - \frac{iV\epsilon}{2\sqrt{N}} J_x (A - A^*) - \gamma \left( J_z + \frac{N}{2} \right) \quad (\text{A.26})$$

$$\dot{A} = \langle \dot{\hat{a}} \rangle = i \langle [H, \hat{a}] \rangle \quad (\text{A.27})$$

$$= i \left\langle \left[ \sum_{j=1}^N \left[ \frac{V}{2\sqrt{N}} [(2+\epsilon) \hat{\sigma}_{x,j} - i\epsilon \hat{\sigma}_{y,j}] \hat{a}^\dagger \right] + \omega \hat{a}^\dagger \hat{a}, \hat{a} \right] \right\rangle \quad (\text{A.28})$$

$$= \left\langle \sum_{j=1}^N \left[ -\frac{iV}{2\sqrt{N}} [(2+\epsilon) \hat{\sigma}_{x,j} - i\epsilon \hat{\sigma}_{y,j}] \right] - i\omega \hat{a} \right\rangle \quad (\text{A.29})$$

$$= -\frac{iV}{2\sqrt{N}} ((2+\epsilon) J_x - i\epsilon J_y) - i\omega A \quad (\text{A.30})$$

All of the equations of motion are collected here:

$$\dot{A} = -\frac{iV}{2\sqrt{N}} ((2 + \epsilon)J_x - i\epsilon J_y) - i\omega A \quad (\text{A.31})$$

$$\dot{J}_x = -\frac{\omega_0}{2} J_y + \frac{iV\epsilon}{2\sqrt{N}} J_z (A - A^*) - \frac{\gamma}{2} J_x \quad (\text{A.32})$$

$$\dot{J}_y = -\frac{\Omega}{2} J_z + \frac{\omega_0}{2} J_x - \frac{V}{2\sqrt{N}} J_z (2 + \epsilon) (A + A^*) - \frac{\gamma}{2} J_y \quad (\text{A.33})$$

$$\dot{J}_z = \frac{\Omega}{2} J_y + \frac{V}{2\sqrt{N}} J_y (2 + \epsilon) (A + A^*) - \frac{iV\epsilon}{2\sqrt{N}} J_x (A - A^*) - \gamma \left( J_z + \frac{N}{2} \right) \quad (\text{A.34})$$

# Appendix B

## Fluctuations around the mean

So far a mean field approach has been used. It is interesting to investigate the fluctuations around the mean in order to get an understanding of the system's stability. In this section the noise is assumed to be linear around the mean and a linearization of the noise is made followed by a diagonalization of the matrix describing the time evolution. The formal way to describe the time evolution is

$$\bar{v} = \mathbb{M} \cdot \bar{v}, \quad (\text{B.1})$$

where  $\bar{v}$  is a vector representing the fluctuations around the mean of the collective spin operators  $\{J_i, A\}$  and  $\mathbb{M}$  is the matrix describing the time evolution.

### B.1 Linearization of the noise

An operator can be written as an expectation value and its fluctuations around it

$$\hat{O} = O + \delta\hat{O}, \quad (\text{B.2})$$

where  $\hat{O}$  is the operator,  $O$  the expectation value and  $\delta\hat{O}$  is the fluctuation. If one take the derivative of this equation with regards to  $t$  one obtains

$$\frac{d\hat{O}}{dt} = \frac{dO}{dt} + \frac{d\delta O}{dt} \quad (\text{B.3})$$

which enables one to get an equation of the time derivative of the fluctuations

$$\frac{d\delta O}{dt} = \frac{d\hat{O}}{dt} - \frac{dO}{dt}. \quad (\text{B.4})$$

In the following the noise operators  $\delta\hat{A}$  and  $\delta\hat{J}_i$  will be deduced.

## B.2 $\delta\hat{A}, \delta\hat{A}^*$ -terms

According to equation (B.2) the  $\hat{A}$ -operator can be expressed as

$$\hat{A} = A + \delta\hat{A} \quad (\text{B.5})$$

and the time derivative of the noise as

$$\frac{d\delta\hat{A}}{dt} = \frac{d\hat{A}}{dt} - \frac{dA}{dt}. \quad (\text{B.6})$$

If one chooses  $\frac{dA}{dt}$  to be

$$\frac{dA}{dt} = -\frac{iV}{2\sqrt{N}} [(2 + \epsilon) J_x - i\epsilon J_y] - i\omega A \quad (\text{B.7})$$

equation (B.6) reduces to

$$\frac{d\delta\hat{A}}{dt} = -\frac{iV}{2\sqrt{N}} [(2 + \epsilon) \delta\hat{J}_x - i\epsilon\delta\hat{J}_y] - i\omega\delta\hat{A} \quad (\text{B.8})$$

and  $\frac{d\delta\hat{A}^*}{dt}$  is hence given by

$$\frac{d\delta\hat{A}^*}{dt} = \frac{iV}{2\sqrt{N}} [(2 + \epsilon) \delta\hat{J}_x + i\epsilon\delta\hat{J}_y] + i\omega\delta\hat{A}^* \quad (\text{B.9})$$

## B.3 $\delta\hat{J}_i$ -terms

### B.3.1 $\delta\hat{J}_x$ -term

According to equation (B.2) the  $\hat{J}_x$ -operator can be expressed as

$$\hat{J}_x = J_x + \delta\hat{J}_x \quad (\text{B.10})$$

and the time derivative of the noise as

$$\frac{d\delta\hat{J}_x}{dt} = \frac{d\hat{J}_x}{dt} - \frac{dJ_x}{dt}. \quad (\text{B.11})$$

If one chooses  $\frac{dJ_x}{dt}$  to be

$$\frac{dJ_x}{dt} = -\frac{\omega_0}{2}J_y + \frac{iV\epsilon}{2\sqrt{N}}J_z(A - A^*) - \frac{\gamma}{2}J_x \quad (\text{B.12})$$

equation (B.11) equals

$$\frac{d\delta\hat{J}_x}{dt} = -\frac{\omega_0}{2}\delta\hat{J}_y + \frac{iV\epsilon}{2\sqrt{N}}\delta\hat{J}_z(A - A^*) + \frac{iV\epsilon}{2\sqrt{N}}J_z(\delta\hat{A} - \delta\hat{A}^*) - \frac{\gamma}{2}\delta\hat{J}_x \quad (\text{B.13})$$

### B.3.2 $\delta\hat{J}_y$ -term

According to equation (B.2) the  $\hat{J}_y$ -operator can be expressed as

$$\hat{J}_y = J_y + \delta\hat{J}_y \quad (\text{B.14})$$

and the time derivative of the noise as

$$\frac{d\delta\hat{J}_y}{dt} = \frac{d\hat{J}_y}{dt} - \frac{dJ_y}{dt}. \quad (\text{B.15})$$

If one chooses  $\frac{dJ_y}{dt}$  to be

$$\frac{dJ_y}{dt} = -\frac{\Omega}{2}J_z + \frac{\omega_0}{2}J_x - \frac{V}{2\sqrt{N}}J_z(2 + \epsilon)(A + A^*) - \frac{\gamma}{2}J_y \quad (\text{B.16})$$

equation (B.15) equals

$$\frac{d\delta\hat{J}_y}{dt} = -\frac{\Omega}{2}\delta\hat{J}_z + \frac{\omega_0}{2}\delta\hat{J}_x - \frac{V}{2\sqrt{N}}\delta\hat{J}_z(2 + \epsilon)(A + A^*) - \frac{V}{2\sqrt{N}}J_z(2 + \epsilon)(\delta\hat{A} + \delta\hat{A}^*) - \frac{\gamma}{2}\delta\hat{J}_y \quad (\text{B.17})$$

### B.3.3 $\delta\hat{J}_z$ -term

According to equation (B.2) the  $\hat{J}_z$ -operator can be expressed as

$$\hat{J}_z = J_z + \delta\hat{J}_z \quad (\text{B.18})$$

and the time derivative of the noise as

$$\frac{d\delta\hat{J}_z}{dt} = \frac{d\hat{J}_z}{dt} - \frac{dJ_z}{dt}. \quad (\text{B.19})$$

If one chooses  $\frac{dJ_z}{dt}$  to be

$$\frac{dJ_z}{dt} = \frac{\Omega}{2}J_y + \frac{V}{2\sqrt{N}}J_y(2+\epsilon)(A+A^*) - \frac{iV\epsilon}{2\sqrt{N}}J_x(A-A^*) - \gamma\left(J_z + \frac{N}{2}\right) \quad (\text{B.20})$$

equation (B.19) equals

$$\frac{d\delta\hat{J}_z}{dt} = \frac{\Omega}{2}\delta\hat{J}_y + \frac{V}{2\sqrt{N}}\delta\hat{J}_y(2+\epsilon)(A+A^*) + \frac{V}{2\sqrt{N}}J_y(2+\epsilon)(\delta\hat{A} + \delta\hat{A}^*) \quad (\text{B.21})$$

$$- \frac{iV\epsilon}{2\sqrt{N}}\delta\hat{J}_x(A-A^*) - \frac{iV\epsilon}{2\sqrt{N}}J_x(\delta\hat{A} - \delta\hat{A}^*) - \gamma\delta\hat{J}_z \quad (\text{B.22})$$

## B.4 Summary

The time derivative of the fluctuations of the mean values are given in the equations below.

$$\frac{d\delta\hat{A}}{dt} = -\frac{iV}{2\sqrt{N}} \left[ (2+\epsilon)\delta\hat{J}_x - i\epsilon\delta\hat{J}_y \right] - i\omega\delta\hat{A} \quad (\text{B.23})$$

$$\frac{d\delta\hat{A}^*}{dt} = \frac{iV}{2\sqrt{N}} \left[ (2+\epsilon)\delta\hat{J}_x + i\epsilon\delta\hat{J}_y \right] + i\omega\delta\hat{A}^* \quad (\text{B.24})$$

$$\frac{d\delta\hat{J}_x}{dt} = -\frac{\omega_0}{2}\delta\hat{J}_y + \frac{iV\epsilon}{2\sqrt{N}}\delta\hat{J}_z(A-A^*) + \frac{iV\epsilon}{2\sqrt{N}}J_z(\delta\hat{A}-\delta\hat{A}^*) - \frac{\gamma}{2}\delta\hat{J}_x \quad (\text{B.25})$$

$$\begin{aligned} \frac{d\delta\hat{J}_y}{dt} = & -\frac{\Omega}{2}\delta\hat{J}_z + \frac{\omega_0}{2}\delta\hat{J}_x - \frac{V}{2\sqrt{N}}\delta\hat{J}_z(2+\epsilon)(A+A^*) \\ & - \frac{V}{2\sqrt{N}}J_z(2+\epsilon)(\delta\hat{A}+\delta\hat{A}^*) - \frac{\gamma}{2}\delta\hat{J}_y \end{aligned} \quad (\text{B.26})$$

$$\begin{aligned} \frac{d\delta\hat{J}_z}{dt} = & \frac{\Omega}{2}\delta\hat{J}_y + \frac{V}{2\sqrt{N}}\delta\hat{J}_y(2+\epsilon)(A+A^*) + \frac{V}{2\sqrt{N}}J_y(2+\epsilon)(\delta\hat{A}+\delta\hat{A}^*) \\ & - \frac{iV\epsilon}{2\sqrt{N}}\delta\hat{J}_x(A-A^*) - \frac{iV\epsilon}{2\sqrt{N}}J_x(\delta\hat{A}-\delta\hat{A}^*) - \gamma\delta\hat{J}_z \end{aligned} \quad (\text{B.27})$$

# Appendix C

## MATLAB programs

# Bibliography

- [1] W. Paul: "*Ein neues massenspektrometer ohne magnetfeld*", Zeitschrift für naturforschung, A8, 448-450 (1953)
- [2] C. Foot: "*Atomic Physics*", Oxford, University Press (2005)
- [3] J. I. Cirac and P. Zoller: "*Quantum Computations with Cold Trapped Ions*", Phys. Rev. Lett. 74, 4091 (1995)
- [4] C. Monroe, D. M. Meekhof, B. E. King, W. M. Itano, and D. J. Wineland: "*Demonstration of a Fundamental Quantum Logic Gate*", Phys. Rev. Lett. 75, 4714 (1995)
- [5] K. Hepp and E.H. Lieb: "*On the superradiant phase transition for Molecules in a Quantized Radiation Field: Dicke Maser Model*", Annals of Physics 76: 360-404 (1973)
- [6] L. D. Landau and E. M. Lifschitz: "*Statistical Physics*", Course of Theoretical Physics, Vol. 5, Pergamon, London, England (1999)
- [7] S. Sachdev: "*Quantum Phase Transition*", Cambridge University Press, Cambridge, England (1999)
- [8] F. Dimer, et.al: "*Proposed realization of the Dicke-model quantum phase transition in an optical cavity QED system*", Physical reviews A 75, 013804 (2007)
- [9] M. J. Bhaseen, J. Mayoh, B. D. Simons and J. Keeling: "*Dynamics of nonequilibrium Dicke models*", Physical review A 85, 013817 (2012)
- [10] D. Nagy, et.al: "*Critical exponent of a quantum-noise-driven phase transition: The open-system Dicke model*", Physical review A 84, 043637 (2011)
- [11] L. D. Landau: , Z, Sowjetunion, 11, 26 (1937)

- [12] F. Reiter, A. Sørensen: "*Effective operator formalism for open quantum systems*", Phys. Rev. A 85, 032111 (2012)
- [13] D.J. Griffiths: "*Introduction to Quantum Mechanics*", Pearson Education, Inc, 2nd edition (2005)
- [14] Knight, et.al: "*Introduction to Quantum Optics*", Oxford, University Press (2005)
- [15] A. Sørensen: "*Lecture Notes for Quantum Optics 2*", Not published (2013)
- [16] P.A.M Dirac: "*The Quantum Theory of the Emission and Absorption of Radiation*", Proceedings of the Royal Society of London, A 114, 243 (1927)
- [17] A. Sørensen: "*Introduction to ion traps*", Not published (2006)
- [18] K. Hammerer, A.S. Soerensen and E.S. Polzik: "*Quantum Interface between light and atomic ensembles*", Rev. Mod. Physics 82, 1041 (2010)
- [19] N.G. van Kampen: "*Stochastic Processes in Physics and Chemistry*", Elsevier, Third Edition (2007)
- [20] Barry M. Garraway: "*The Dicke model in quantum optics: Dicke model revisited*", Phil. Trans. R. Soc. A 2011 369 (2011)
- [21] D. Leibfried, R. Blatt, C. Monroe, et al.: "*Quantum dynamics of single trapped ions*", Reviews of modern physics, volume 75 (2003)
- [22] P. Cappallaro: "*Quantum Theory of Radiation Interactions*" Fall 2012, MIT
- [23] S. Morrison and A. S. Parkins: "*Collective spin systems in dispersive optical cavity QED: Quantum phase transitions and entanglement*", Phys. Rev. A 77, 043810 (2008)
- [24] L.J. Zou, D. Marcos, S. Diehl, S. Putz, J. Schmiedmayer, J. Majer and P. Rabl: "*Implementation of the Dicke lattice model in hybrid quantum system arrays*", Phys. Rev. Lett. 113, 023603 (2014)
- [25] S. Genway, et.al: "*Nonequilibrium Dynamics in Trapped Ions*", Physical reviews letters, PRL 112, 023603 (2014)
- [26] G. Morigi and H. Walther: "*Two-species coulomb chains for quantum information*", Euro. Phys. J. D, 13, 261-269 (2001)

- [27] H.J Metcalf and P. v.d. Straten: "*Laser Cooling and Trapping*", Springer-verlag New York, Inc (1999)